Optimized Monophasic Pulses with Equivalent Electric Field for Rapid-Rate Transcranial Magnetic Stimulation

Boshuo Wang[1], Jinshui Zhang[2], Zhongxi Li[2], Warren M. Grill[2,3,4,5], Angel V. Peterchev[1,2,3,4], Stefan M. Goetz[1,2,4,6*]

[1] Department of Psychiatry and Behavior Sciences, School of Medicine, Duke University, Durham, NC, USA

[2] Department of Electrical and Computer Engineering, School of Engineering, Duke University, Durham, NC, USA

[3] Department of Biomedical Engineering, School of Engineering, Duke University, Durham, NC, USA

[4] Department of Neurosurgery, School of Medicine, Duke University, NC, USA

[5] Department of Neurobiology, School of Medicine, Duke University, NC, USA

[6] Department of Engineering, School of Technology, University of Cambridge, Cambridge, UK

[*] Corresponding author: stefan.goetz@duke.edu, smg84@cam.ac.uk

Keywords: transcranial magnetic stimulation, pulse shape, waveform optimization, coil heating, pulse energy

Abstract

Objective. Transcranial magnetic stimulation (TMS) with monophasic pulses achieves greater changes in neuronal excitability but requires higher energy and generates more coil heating than TMS with biphasic pulses, and this limits the use of monophasic pulses in rapid-rate protocols. We sought to design a stimulation waveform that retains the characteristics of monophasic TMS but significantly reduces coil heating, thereby enabling higher pulse rates and increased neuromodulation effectiveness.

Approach. A two-step optimization method was developed that uses the temporal relationship between the electric field (E-field) and coil current waveforms. The optimization step reduced the ohmic losses of the coil current and constrained the error of the E-field waveform compared to a template monophasic TMS pulse, with pulse duration as a second constraint. The second, amplitude adjustment step scaled the candidate waveforms based on simulated neural activation to account for differences in stimulation thresholds. The optimized waveforms were implemented to validate the changes in coil heating.

Main results. Depending on the pulse duration and E-field matching constraints, the optimized waveforms produced 12% to 75% less heating than the original monophasic pulse. The results were robust across a range of neural models. The changes in the measured ohmic losses of the optimized pulses compared to the original pulse agreed with numeric predictions.

Significance. The first step of the optimization approach was model-free and exhibited robust performance by avoiding the highly non-linear behavior of neural responses, while neural simulations were only run once for amplitude scaling in the second step. This significantly reduced computational cost compared to iterative methods using large populations of candidate solutions and reduced the sensitivity to choice of neural model. The reduced coil heating and power losses of the optimized pulses can enable rapid-rate monophasic TMS protocols.

1. Introduction

Magnetic stimulation is a noninvasive technique to activate neurons. Transcranial magnetic stimulation (TMS) is used to probe and modulate brain function [1,2] and clinical TMS routinely serves for the diagnosis and treatment of psychiatric and neurological disorders [3,4]. The technique uses an electromagnetic coil to generate an intense time-varying magnetic field of about one tesla to induce an electric field (E-field) in the brain [5]. Various TMS waveforms and pulse directions recruit different neural targets and achieve different levels of changes in excitability [6–10]. For instance, repetitive TMS with monophasic pulses generates stronger facilitation and activates cortical neurons with higher directional selectivity [11–15], but clinical applications almost exclusively use biphasic pulses.

The reasons for exclusive use of biphasic pulses in repetitive TMS are mostly technical. Due to the weak electromagnetic coupling, TMS requires currents and voltages of several kiloamperes and kilovolts [16–19], which generate rapid coil heating during repetitive pulse trains. As safety regulations limit the temperature of the coil surface in contact with the subject [20], most coils for repetitive stimulation require complex cooling systems but still have heating-related restrictions on the pulse strength, rate, and/or number. As the least energy-efficient pulse shape, monophasic pulses cannot operate at high repetition rates due to the excessive power loss. This power loss causes heating in the coil and the hardware needs a sufficient power supply to provide this power. Biphasic pulses, despite producing weaker facilitation and being less selective, can be generated more efficiently, cause less heating, and therefore allow higher repetition rates [21,22].

For example, quadripulse stimulation (QPS) with four monophasic pulses delivered in a rapid sequence [23] creates the largest [24–26] and most repeatable [27,28] changes in excitability, but is typically performed with low burst repetition rate such as 0.2 Hz [29,30]. QPS using higher burst rate (e.g., ~ 5 Hz) appears to retain its efficacy with just a fraction of the stimulation session duration [31,32]; however, such a protocol has only been demonstrated with the less effective but more energy efficient biphasic pulses. Similarly, theta-burst stimulation with monophasic pulses is currently not possible. Present commercial devices cannot generate any of the approved treatment protocols for major depression with monophasic pulses which require pulse rates of at least 10 Hz [33–35], and all medical treatments use biphasic pulses despite the resulting smaller changes in excitability. Repetitive TMS could be significantly improved with a pulse shape that produces changes in excitability equivalent to those produced by a monophasic pulse and but with higher energy efficiency.

The high power requirements of TMS devices and associated demands on the underlying electronic circuits and passive components are a key reason for the slow technological development of pulse sources that allow control of the pulse waveform [21]. Therefore, minimization of the energy required to generate specific E-field waveforms is advantageous. Previous theoretical optimization with nonlinear neuron models suggested that the pulse power and coil heating could be reduced by more than a factor of two [36]. However, the reported pulses are more bidirectional than conventional monophasic pulses and bear no close resemblance with any conventional or clinically approved pulse shape, and thus it is not clear that they could produce equivalent changes in excitability.

Several TMS technologies allow increased waveform flexibility [37–44], but pulse shapes that are both highly efficient with low coil heating and replicate accurately the E-field waveform of monophasic pulses have not been implemented. Herein we design pulse shapes that produce estimated neural activation equivalent to conventional monophasic pulses by matching the induced E-field but with minimized pulse power and coil heating. We introduce a novel model-free optimization approach, and non-linear models are introduced only for amplitude adjustment, thereby reducing substantially the computational demands and sensitivity to model selection.

2. Method

2.1. Optimization Rationale and Overview

Unlike electrical stimulation, the temporal waveform of the TMS E-field, $E(t)$, and current density induced in the tissue is not directly proportional to the output current generated by the TMS device, $I_{\mathrm{coil}}(t)$, but rather proportional to its time derivative [45] (see Supplementary Materials for more discussion):

$$E(t) \propto \frac{\mathrm{d}I_{\mathrm{coil}}(t)}{\mathrm{d}t} \quad . \tag{1}$$

Therefore, a slow shift in the baseline of the coil current I_{coil} before the pulse minimally affects the induced E-field but reduces the energy loss, W, [36], which is mostly in the form of ohmic heating of the coil, its cable, and other circuit components in series with the coil per

$$W = R_{\mathrm{coil}} \int I_{\mathrm{coil}}^2 \cdot \mathrm{d}t \quad , \tag{2}$$

where R_{coil} is the total resistance. Specifically, for monophasic TMS pulses with unidirectional I_{coil}, shifting the entire waveform reduces the peak amplitude of I_{coil} and W. Through a tightly enforced shape similarity of the resultant E-field, the optimized pulse should have similar stimulation effects compared to the monophasic TMS pulse (Figure 1A), and preserve stimulation characteristics of the latter, such as directional selectivity and motor activation latency [8,46].

We set up a free optimization, where loss-reducing features of the current waveform can evolve just through the objective and the constraints without introducing any features a-priori. The optimization problem is separated into two steps. The first step is formulated as a classic optimization problem that focuses on modification of the waveform shape; the second step deploys neural models to adjust the waveform amplitude to account for minor shifts of the activation threshold that might arise from the first step (Figure 1B).

2.2. Two-Step Optimization

The optimization problem starts with the coil current I_{coil} and the E-field E of the conventional TMS monophasic pulse shape. We used an E-field waveform recorded from a MagPro X100 device (MagVenture A/S, Farum, Denmark), which is normalized to one (V/m) at the pulse start, and calculated the corresponding coil current (in arbitrary units) as the integral (cumulative sum) of the E-field waveform. (Half-sine and biphasic pulses of the

same TMS device were also utilized for comparison.) The optimization algorithm uses a sequential quadratic programming method, implemented with the MATLAB function fmincon, and works on I_{coil} with either the original monophasic pulse or random Gaussian noise as the starting point, and minimizes the cost function W (with R_{coil} set to unity). To ensure minimal effect on the E-field and subsequent neural activation, the main optimization constraint is the root-mean-square error (RMSE) of the E-field waveform compared to the original TMS template waveform. We performed optimization with five RMSE levels: 0.25%, 0.5%, 1%, 2%, and 4% of the peak E-field amplitude. Constraints are also imposed at the beginning and the end of the pulse, so that I_{coil} starts from and returns to zero. Thus, the pulse current has a mathematically compact support, which ensures a finite pulse duration and avoids any unaccounted pulse energy or loss. For computational optimization purposes, the waveforms are sampled with a 10 µs time step. This temporal sampling turned out to be sufficient as doubling the sampling (5 µs time step) did not affect the optimization (Figure S2A).

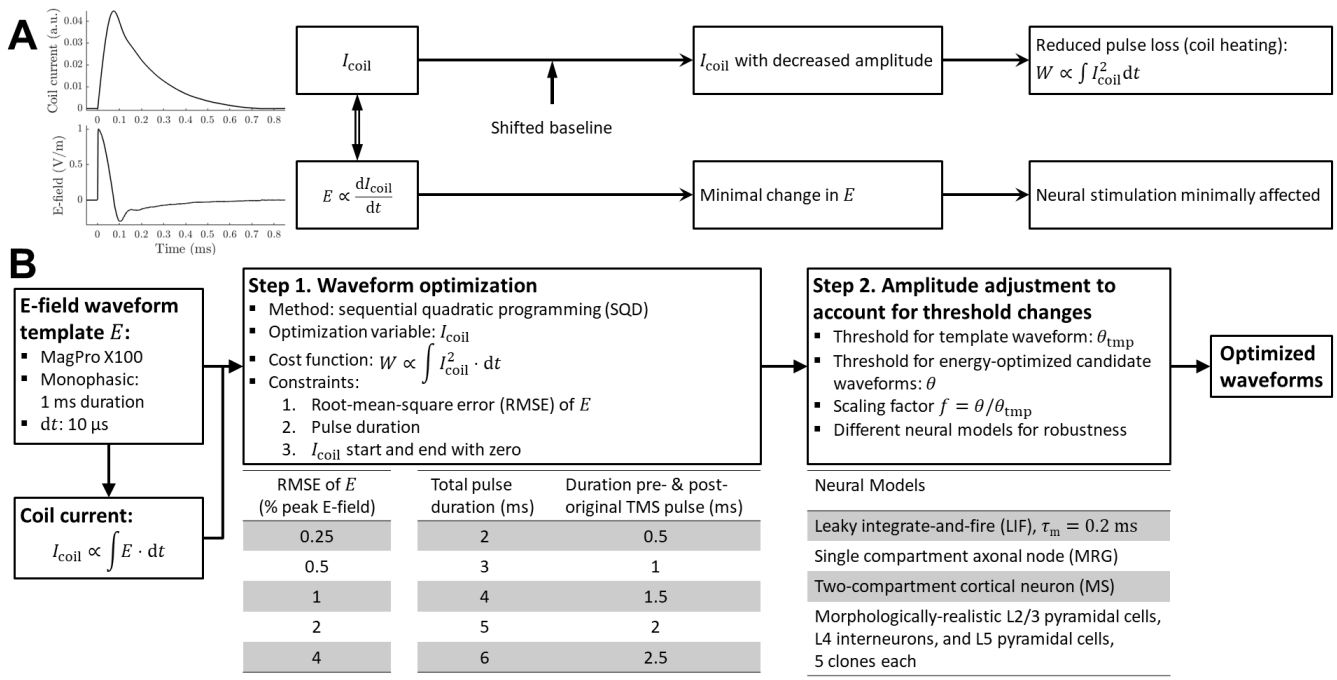

Figure 1: Waveform optimization principle and steps

A. The waveform optimization used the relationship between the TMS-induced E-field waveform E and coil current I_{coil}. A shifted baseline reduces the amplitude of the current waveform and ohmic losses, whereas the E-field waveform and its stimulation effect is only minimally affected. **B**. The optimization starts with an E-field waveform template and in the first step produces a corresponding current waveform with minimal heating while limiting the error of the E-field compared to the template. In the second step, the amplitude of the candidate waveforms is scaled to account for differences in neural activation thresholds introduced during the first step. MRG: McIntyre-Richardson-Grill model. MS: Mainen-Sejnowski model.

Another constraint in the optimization is the duration of the optimized pulse, which—together with the RMSE constraint—determines how long before and after the reference pulse additional features can evolve. For example, a low-amplitude, slow-changing leading phase that shifted the current baseline before the depolarizing main phase emerged in our prior work on pulse optimization without shape constraints [36]. The original TMS current pulse has a duration of approximately 0.75 ms due to the long current decay, whereas the dominant phase of the E-field is only about 75 μs long (Figure 1A). We extended (zero-padded) the original TMS pulse (set to 1 ms total duration) both before and after with five durations between 0.5 ms to 2.5 ms, resulting in a total pulse duration in the range of 2 to 6 ms. These pulse durations corresponded to 201 to 601 time points for I_{coil} and E. A desktop computer (with an Intel Core i7-8700 CPU and 16 GB RAM) performed each optimization condition independently up to ten times to examine the consistency of the results and the runtime. Computation and data analysis were performed with MATLAB (version 2021a, The Mathworks, Natick, MA, USA).

The second step in the design process scales the amplitude of the candidate waveforms to the stimulation threshold in neural models. We administered the E-field waveforms of the original TMS template and the candidate waveforms to neuron models and obtained their respective stimulation thresholds θ_{tmp} and θ within 0.1% accuracy using a binary search. To allow sufficient time for the stimulation to evoke an action potential, the simulations were extended by 6.5 to 8.5 ms depending on the total duration of the pulse. For accurate simulation of the neural thresholds, the stimulation waveforms were linearly interpolated with a time step of 2.5 μs. We scaled the amplitude of each candidate waveform by their corresponding factor

$$f = \theta/\theta_{\mathrm{tmp}} \tag{3}$$

to form the optimized threshold-matched waveforms. We quantified the change in loss of the threshold-matched pulses as a percentage of the original monophasic pulse

$$\eta = \frac{W - W_{\mathrm{tmp}}}{W_{\mathrm{tmp}}} \times 100\% \quad . \tag{4}$$

2.3. Neuron models

Several neural models were used to assess the robustness of the second, amplitude adjustment step. The first model was a single-compartment linear leaky integrate-and-fire (LIF) model. A time constant of 200 μs was chosen based on experimental neural responses to TMS [43,47,48]. The second was a single compartment model (MRG, McIntyre-Richardson-Grill) of a peripheral axon node [36,49]. The third was a two-compartment model (MS, Mainen-Sejnowski) that replicated firing pattern of cortical neurons with realistic dendrite morphology [50,51]. An intracellular current injection proportional to the E-field waveform stimulated these models, which were simulated in MATLAB on the same desktop computer that performed the optimization.

The remaining models were 15 morphologically-realistic cortical neuron models from the Blue Brain project [52] adapted for studying brain stimulation in the human cortex [46,53], including layer 2/3 pyramidal cells (PC), layer 4 interneurons, and layer 5 PCs, with five morphological clones used for each layer. The simulations were set

up in MATLAB and performed in NEURON (version 7.7) [54] on the Duke Compute Cluster. The extracellular stimulation was applied using quasi-uniform approximation of the E-field [55]. E-field orientations were sampled in a spherical coordinate system in which the *z*-axis aligned with the somatodendritic axis [46,56], with 13 polar angles in [0°, 180°] (average spacing of 15°), 18 azimuthal angles in [0°, 360°) (spacing of 20°), and a total of 200 (11×18+2) orientations. Amplitude adjustment factors were calculated for all 5000 (200×5×5) combinations of orientations and candidate waveforms.

2.4. Experimental waveform implementation

A modular pulse synthesizer TMS (MPS-TMS) device (Figure S1A) with six modules [40] was used to generate the optimized pulses. All waveforms were normalized to the maximum peak value and interpolated using a 5 MHz sampling rate. Before each pulse delivery, the internal capacitors of the modules (3.986 mF per module) were charged to 75 V, which generated output voltage between −450 V and 450 V. Despite the capacitors being disconnected from the dc power supply during the pulse, the control algorithm compensated for the voltage drop to maintain the correct amplitude of the current delivered.

A custom minimum-energy figure-of-8 coil following a previous design [57] served as the test coil for the pulses (Figure S2B). The coil had an inductance L_{coil} of 9.46 μH and resistance R_{coil} of 11.7 mΩ at 1 kHz, measured in four-wire configuration with an LCR/ESR meter (Model 889A, B&K Precision Corporation, USA). Electrical measurements were performed with a 500 MHz oscilloscope (Tektronix MDO3054, Beaverton, OR, USA) and high-voltage differential probes (Tektronix THDP0100) and a Rogowski current transducer (CWT 60B, Power Electronic Measurement Ltd., Nottingham, UK) to measure the coil voltage and current, respectively, at 100 MHz sampling frequency (Figure S2C). The module voltage V_{DC} was also measured from the modules' dc capacitors after each pulse. A 70-mm-high printed-circuit-board-based triangular probe [58,59] measured the E-field corresponding to a depth of 15 mm under the center of the coil in an 85 mm sphere approximating the head (Figure S2B). For visualization only, a 3rd-order Butterworth low-pass filter with a cut-off frequency of 100 kHz was used to filter the recorded waveforms (with MATLAB function filtfilt) (Figures S6–S9).

The losses for all pulses were calculated from the measurements with three similar metrics: the integral of the coil current squared multiplied by the coil resistance obtained from the LCR/ESR meter measurements (2), the energy based on instantaneous power

$$\widetilde{W} = \int V_{\text{coil}} I_{\text{coil}} \cdot \mathrm{d}t \quad , \tag{5}$$

and the change in the stored energy using the pre- and post-pulse voltage of the device's dc capacitors

$$\widehat{W} = C_{\text{DC}}/2 \cdot (V_{\text{DC,pre}}^2 - V_{\text{DC,post}}^2) \quad , \tag{6}$$

where the total capacitance of all six modules C_{DC} was 23.92 mF and $V_{\text{DC,pre}}$ was 75 V. The first metric captured mostly ohmic heating of the coil; the second included also other losses, such as mechanical vibration of the coil and electromagnetic field radiation; and the third incorporated further switching and operational losses internal to the

MPS-TMS system. The pulse energy, which was the minimum energy required to generate the pulses in the TMS coil, was also calculated using

$$U = L_{\text{coil}} \cdot \max_t \left(I_{\text{coil}}^2 \right) \quad , \tag{7}$$

which corresponded to the peak magnetic field energy in the TMS coil, or

$$\widetilde{U} = \max_t \left(\int_{-\infty}^{t} V_{\text{coil}} I_{\text{coil}} \cdot \mathrm{d}t' \right) \quad , \tag{8}$$

which included both the reactive energy U that was provided to the coil and recovered by the device at the end of the pulse and the active power dissipated up to the time of the magnetic field reaching its peak strength.

3. Results

For clarity, the figures in the main text show a subset of the results, e.g., three of the five RMSE constraints, two or three of the five pulse durations, and one or two model clones for each cell type of the Blue Brain models. The full datasets are provided in the supplement.

3.1. Waveform optimization

The optimization generated current waveforms with a negative leading phase that shifted the onset of the main phase toward a more negative baseline. The peak amplitude was decreased and the shape was narrower compared to the original monophasic pulse (Figures 2A and S2B). The magnitude of the leading phase increased and the pulse width and amplitude of the main phase decreased, respectively, with larger RMSE constraint on the E-field waveform and longer pulse duration. The changes in loss compared to the original TMS pulse ranged from −15% to −95% (Figures 2B and S3A, dashed lines in bottom panel of leftmost column). The optimized E-field waveform consisted of a main phase that approximated the original E-field waveform but had a slightly reduced peak amplitude and a negative leading phase with amplitude between −0.4% and −35.4% of the corresponding main peak. Using random initialization of waveforms resulted in the same optimal waveforms (within the optimization tolerance) as initializing with the monophasic TMS pulse.

The second step in the optimization adjusted the amplitude of the optimal waveforms based on the threshold to activate a range of neural models (Figures 2B and S3A). The threshold-based scaling increased the amplitude by ×1.006 for the smallest RMSE and shortest pulse duration constraints up to ×2.71 for the largest RMSE and longest pulse duration constraints. For a given parameter combination of RMSE and pulse duration constraints, the LIF model had the largest amplitude adjustment (×1.02 to ×2.71) and least reduction in heating (−12% to −60%) among all the models. In contrast, all the nonlinear models, regardless of complexity, had smaller amplitude adjustments (×1.006 to ×2.26) and less coil heating (−12% to −81%), which were also highly consistent across the different neuron models. The amplitude adjustment factors f differed by only −0.5% to −17% between the two-compartment MS model and the Blue Brain models, and by −0.5% to −7.4% between the single compartment MRG model and the Blue Brain models, with larger differences for larger RMSE and longer pulse duration constraints.

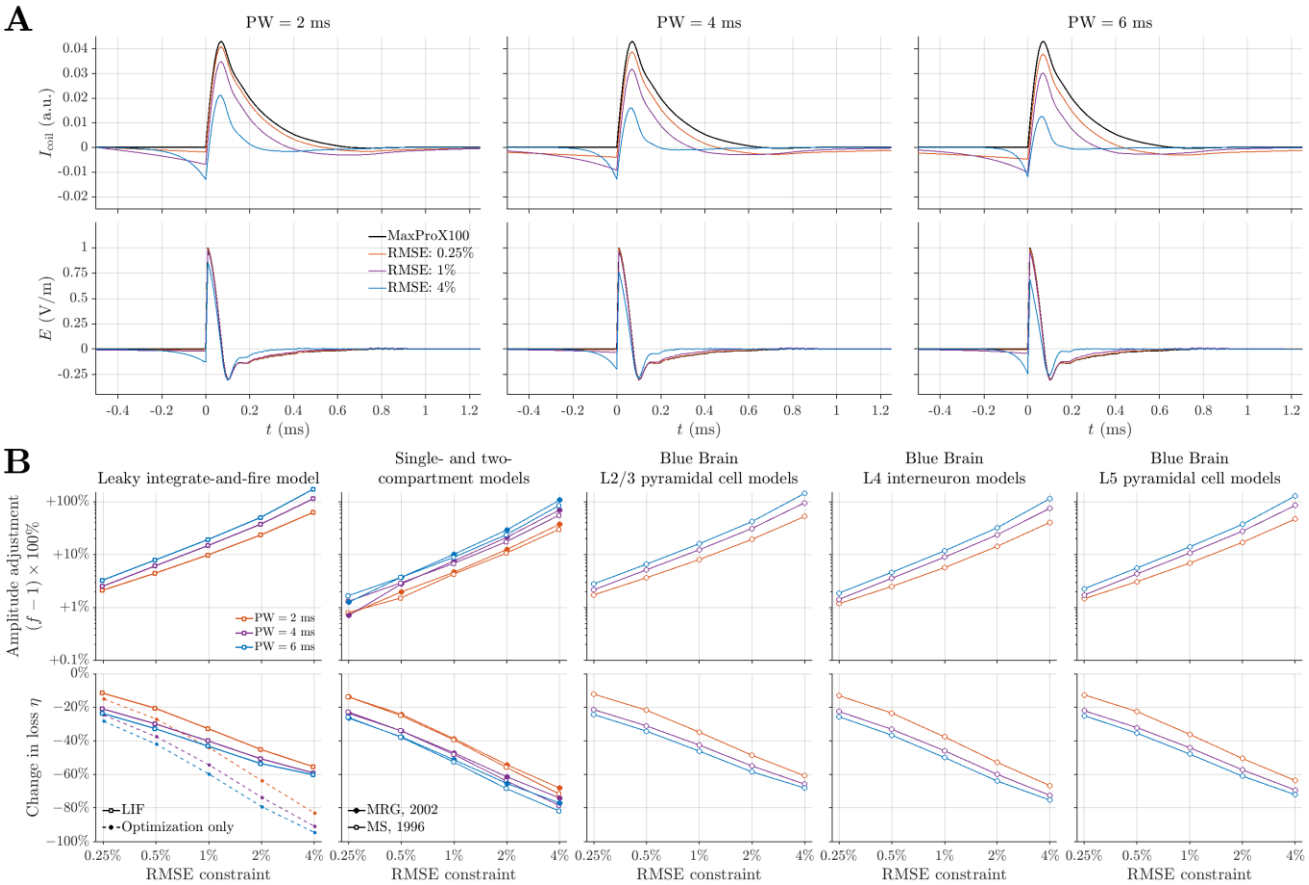

Figure 2: Waveform optimization and amplitude adjustment steps

A. The optimized coil current waveforms (colored lines) had a negative leading phase, reduced amplitude, and narrower shape than the original TMS monophasic pulse (black lines). The corresponding E-field waveforms included a negative leading phase but their main phase resembled the E-field produced by the original pulse. Only the center portion of the optimized waveforms are shown, time-shifted to match the monophasic pulse. **B.** The amplitude adjustment factors f for the optimized waveforms to reach threshold for activation are converted as percentage increase $(f-1)\times 100\%$ and shown on logarithmic scale. They increased with both the total pulse durations and the optimization constraints of the E-field, whereas the loss compared to the original TMS pulse decreased with these parameters. The loss without the amplitude adjustment are also shown in the first column (dashed lines). The results for the Blue Brain models are given for the first model clone for each cell type and are the mean across all the 200 E-field orientations. Full results for all parameters and model clones are given in Figures S2 and S3. PW: pulse width. a.u.: arbitrary units. LIF: leaky integrate-and-fire model. MRG: McIntyre-Richardson-Grill model. MS: Mainen-Sejnowski model.

The coefficients of variation (i.e., ratio of standard deviation to mean) of the amplitude adjustment for individual Blue Brain models (clones) were on the order of 10^{-15} across all 200 E-field orientations for any RMSE and pulse duration constraint. Across the results (15×200) of all 15 models, the coefficient of variation was between 0.1% to

2%, with higher values for larger RMSE and longer pulse duration constraints. The consistency of threshold adjustment across neural models, and especially across E-field orientations for each Blue Brain model, demonstrated that the optimization indeed generated stimulation pulse shapes that have the same characteristics as monophasic TMS pulses, such as directional selectivity. The leading phase of the pulse introduced a delay in neural activation when the action potentials generated by the optimized pulses were compared to those by the conventional monophasic pulse, with the delay equal to the duration the leading phase (i.e., the zero-padding of the original monophasic pulse; Figure S4).The mean amplitude adjustment of the Blue Brain models for each parameter combination was used to scale optimized candidate waveforms to form the final optimized waveforms (Figures 3 (dashed lines in middle and bottom rows) and S3B). With their final RMSE only slightly increased from the corresponding optimization constraints (Figure S5A, on average 0.27%±0.01%, 0.55%±0.01%, 1.13%±0.01%, 2.38%+0.05%, and 5.30%±0.26%, respectively, for 0.25%, 0.5%, 1%, 2%, and 4% RMSE constraint), these waveforms reduced coil heating by 12.5% to 75%. Some of the optimized monophasic pulses exhibited lower losses than conventional biphasic pulses, which already have lower stimulation thresholds [8,46] and less heating compared to conventional monophasic pulses (Figures 4A and S6). For this comparison, we used the biphasic pulses with reversed current direction compared to the monophasic pulse (Figures 4B), which are known to have a lower threshold due to the dominant second phase of the E-field [8,60,61].

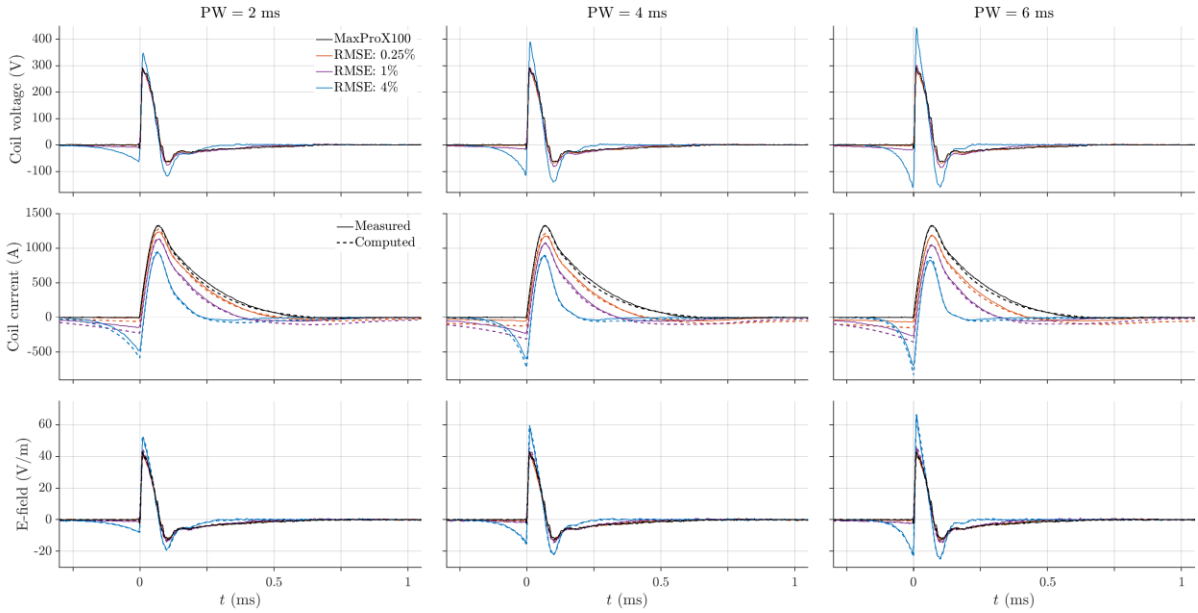

Figure 3: Computed and measured optimized TMS waveforms

The measured coil voltage, the computed (dashed lines) and measured (solid lines) coil currents, and the computed (dashed lines) and measured (solid lines) E-field. The computed current and E-field waveforms were scaled to match the peak of their measured counterparts. Measurements were low-pass filtered for visualization only. Full results for all optimization constraints, the unfiltered waveforms, and the effect of filtering are shown in Figures S8, S9, and S10–S11, respectively. PW: pulse width.

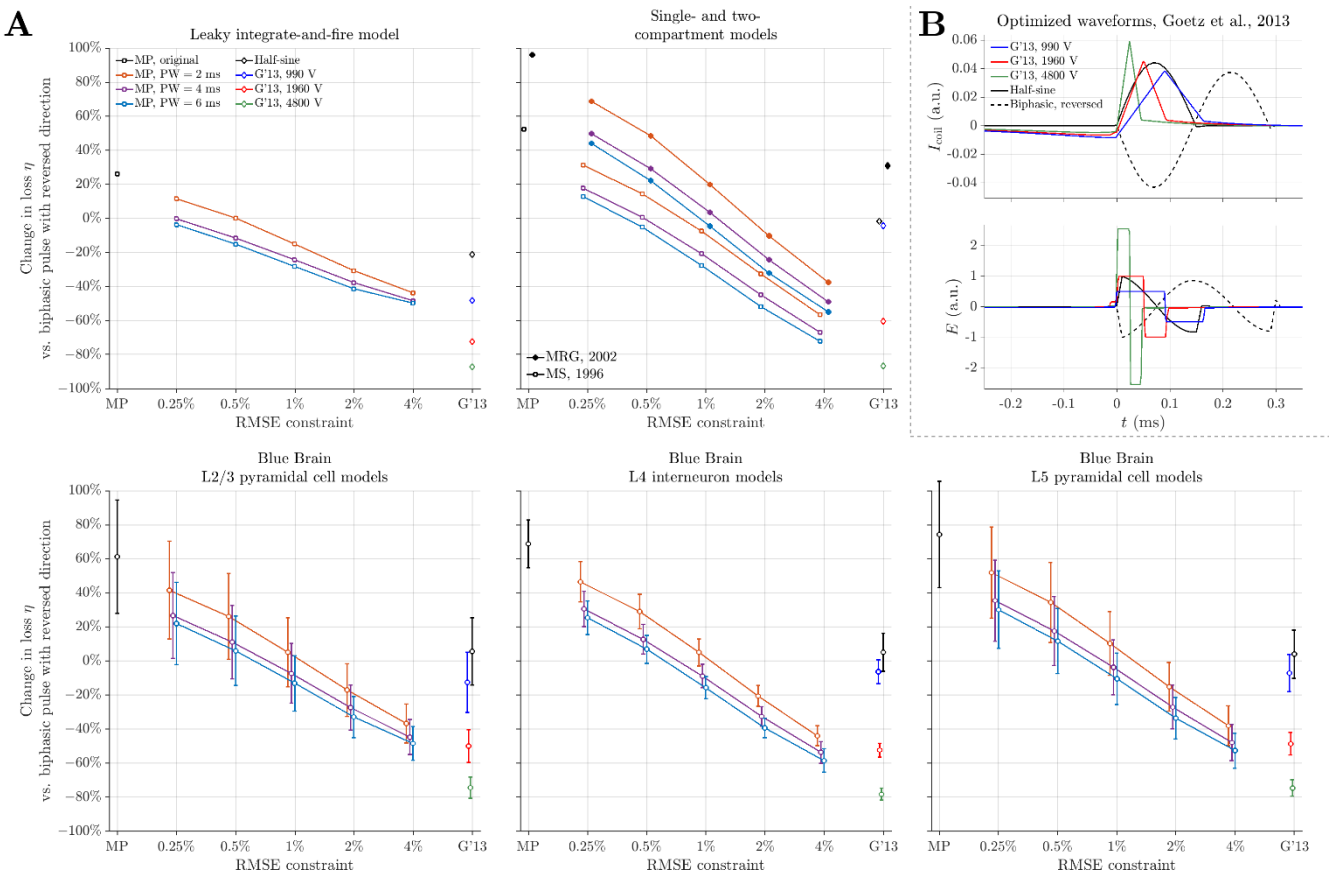

Figure 4: Difference in coil heating comparing pulses with monophasic, optimized, half-sine, and triangular shapes against biphasic pulse

A. The coil heating at stimulation threshold was calculated for a positive pulses for the monophasic (MP) and optimized pulses, as well as half-sine pulse and triangular optimal waveforms (G'13) from previous work [36], and for a negative (reversed) pulses for the biphasic pulse. Similar format as bottom row of Figure 2B. Full results for all pulse durations and model clones are given in Figures S5. PW: pulse width. **B.** Three optimized waveforms from previous work [36] (recreated under the Creative Commons Attribution License), normalized to the second waveform (red line), and conventional half-sine and (reversed) biphasic pulses recorded from MaxPro X100 (black lines). The optimized waveforms have a total duration of 1.6 ms with a 1.2 ms leading phase, with the voltage values indicating the optimization constraint on the coil voltage.

3.2. Computational Runtime

The runtime of the E-field matching optimization step was on the order of a few seconds up to two minutes, with longer runtime for the optimization of longer pulse duration (Figures 5 and S7, solid lines in leftmost column). Doubling and halving the sampling time step from 10 µs to 5 µs and 20 µs changed the optimization time by ×(9.4±2.2) (range ×6.4 to ×13.8) and ÷(7.3±3.1) (range ÷3.5 to ÷14.6), respectively (Figure 5 and S7, dashed and

dotted lines in leftmost column). In comparison, the runtime of the threshold search varied for the different neural models, with single- and two-compartment models requiring < 10 s (Figure 5 and S7, second column) and the morphologically-realistic Blue Brain models (Figure 5 and S7, third to fifth columns) between 1–20 minutes, with one exceptionally complex L4 interneuron model averaging ~ 30 minutes.

3.3. Waveform implementation

The measured waveforms (Figures 3 and S7, solid lines) closely matched the optimized waveforms (Figures 3 and S8, dashed lines) with RMSE in the range between 0.8% and 4% for filtered waveforms and around 4% for all unfiltered results (Figure S5B), indicating successful implementation of the optimized TMS pulses using the MPS-TMS device. The E-field peaked at approximately 66 V/m for the optimal waveform with highest amplitude (4% optimization constraint and 6 ms pulse duration) and at 43 V/m for the original TMS pulse, with corresponding peak coil voltages of 450 V and 292 V, respectively; the coil current, however, was lower for the optimized pulse (peak of 824 A versus 1323 A) due to the negative leading phase (negative peak of −690 V). The optimized waveforms generated less coil heating compared to the original TMS pulse (Figures 6A and S12A), and required less energy to generate the pulse (Figures 6B and S12A). For the various pulses, approximately two thirds of the loss $\widetilde{W}$ was in the form of heat W (66%±6%, range 51%–73%) and the energy efficiency of the MPS-TMS system ($\widetilde{W}/\widehat{W}$) was 51%±2% (range 47%–55%). Despite some deviation likely due to recording noise, the difference of pulse energy calculated from the measurement also matched the prediction by the computation of the optimized waveforms for both the pulse energy and total energy (Figure 6C and 6D, and S12C and S112D).

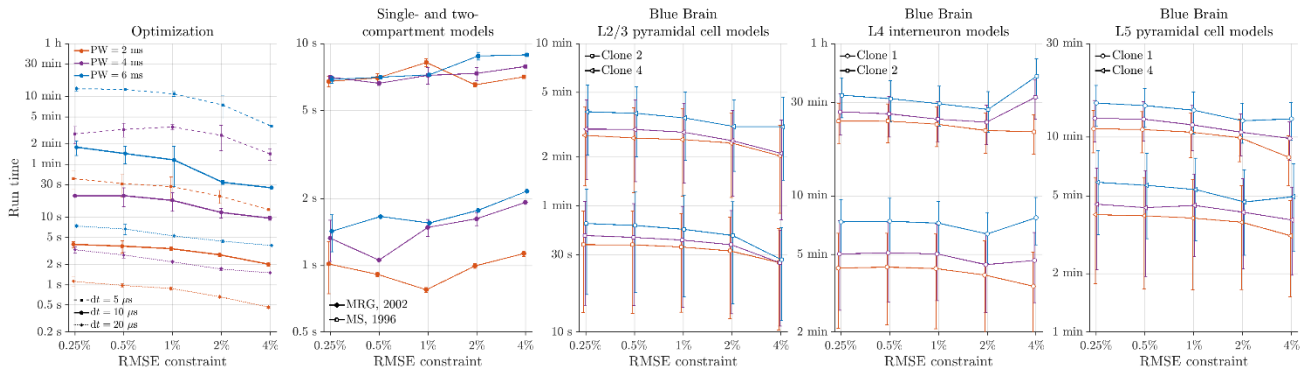

Figure 5: Runtime of optimization and neural simulations

The runtime of the waveform optimization (mean and standard deviation of ten trials for 10 μs and 20 μs time steps, and three trials for 5 μs time step) and threshold search for the single- and two-compartment models (mean and standard deviation of ten trials), and the Blue Brain L2/3 pyramidal cell, L4 interneuron models, and L5 pyramidal cell models (mean and standard deviation of 200 E-field orientations, fastest and slowest clones). The runtime of the LIF model was on the order of milliseconds and not shown. Results for all pulse duration and all model clones are given in Figures S6. PW: pulse width. MRG: McIntyre-Richardson-Grill model. MS: Mainen-Sejnowski model.

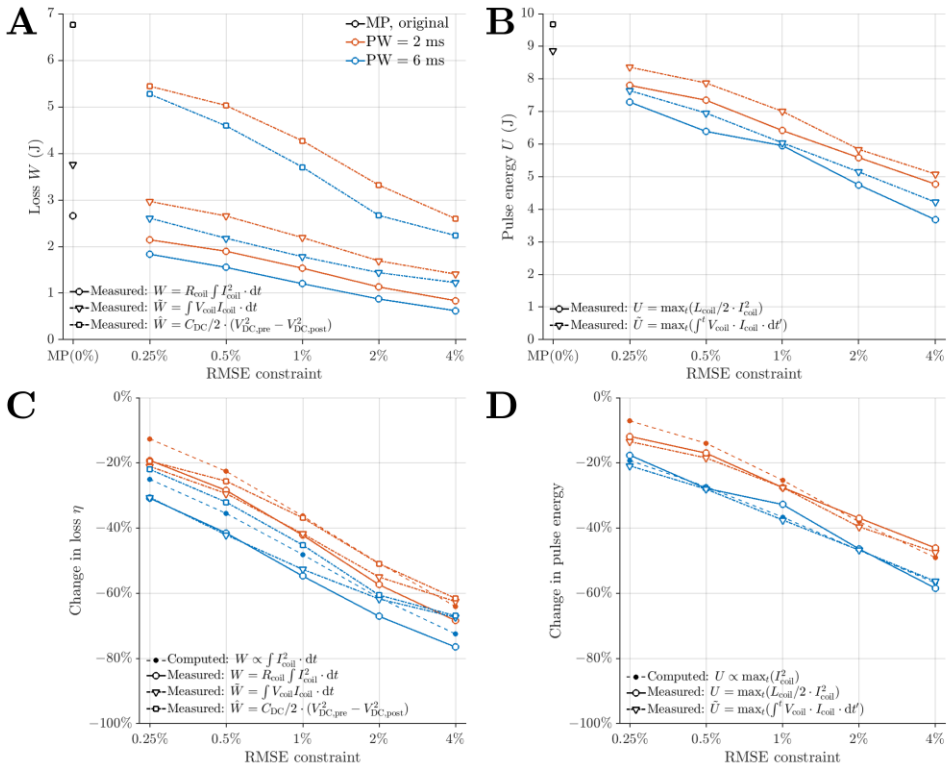

Figure 6: Losses and pulse energy of optimized pulses and original TMS pulse

A. The losses (triangle markers) include the internal losses of the MPS-TMS operation and the energy dissipated through the coil (square markers), which include ohmic heating of the coil (circle markers) as well as other losses. **B.** The total energy required to generate pulses. **C.** The losses of the optimized pulses compared to the original monophasic TMS pulse. **D.** The pulse energy of the optimized pulses compared to the original monophasic TMS pulse. Results for all pulse durations are given in Figures S12. PW: pulse width.

4. Discussion

4.1. Waveform optimization

We utilized a two-step approach to optimize the TMS pulse for minimal coil heating while retaining characteristics of conventional monophasic pulses. In the first step, a classic (i.e., non-heuristic) optimization problem was formulated and solved, which generated optimal waveforms that exhibited a negative prepulse as predicted by the optimization rationale and observed in previous optimization studies [36,62]. It should be noted that the negative leading phase of both the current and E-field were not defined or imposed by the optimization problem itself, but rather was a natural result of the cost function and E-field constraint, as well as the increased pulse duration compared to the monophasic pulse template. As the problem was well-defined and deterministic, the optimization was robust and not subject to random factors such as parameter initialization.

The optimization problem had two constraints, the RMSE of the E-field and the total pulse duration. The deviation of the E-field from the conventional monophasic pulse shape was limited to 0.25% to 4% RMSE during the optimization and the final RMSE after the amplitude adjustment was between 0.27% and 5.6% for computation results and between 0.8% and 4.6% for measurements. Such errors are similar to typical pulse-to-pulse and machine-to-machine variability of common TMS devices [63] and are expected to produce comparable physiological effects below the expected technical tolerance level. The RMSE constraint had a larger influence on the reduction of coil heating compared to the pulse duration (Figures 2B): relaxing the RMSE constraint (higher RMSE) reduced the heating more than increasing the non-zero pulse waveform duration. This was mostly due to higher RMSE resulting in a current waveform that had a main phase with significantly shorter duration and lower amplitude compared to the original TMS pulse, and shorter TMS pulses are known to require less energy and produce less heating [36,47,64,65]. For long pulse durations, further increasing the duration had a diminishing return on the reduction of heating, e.g., increasing pulse duration from 4 ms to 6 ms resulted in a smaller change of coil heating compared to that for pulse duration increased from 2 ms to 4 ms.

The short delay in neural activation introduced by the leading phase and longer pulse duration is not a problem in most TMS applications. When the optimized waveforms are used in place of monophasic pulses in repetitive TMS protocols, most of the leading phase and the prolonged tail of the pulse fall within the interpulse interval—for example, the interstimulus intervals of QPS, theta burst stimulation, or paired pulses are 1.5–100 ms, 20 ms, and in the range from a few up to tens to hundreds of ms, respectively. The delay may have to be considered only for certain applications where sub-millisecond timing is critical, for example phase-specific TMS for a certain electroencephalogram (EEG) rhythm. Still, the delay could be accounted for by prediction algorithms for the EEG phase [66] by triggering the optimized TMS pulse earlier so that the E-field peak aligns with that of a monophasic pulse.

The second optimization step adjusted the waveforms' amplitude based on stimulation thresholds obtained from neural simulations. The linear membrane model, while useful for estimation of time constants [43,46,48], produced significantly higher amplitude adjustment values than the non-linear models since the linear model did not capture the known lowering of threshold by hyperpolarizing negative prepulses due to dis-inhibition of the sodium ion channels [67–71]. The threshold-based scaling factors were consistent across models and cell types that include non-linear ion channels, demonstrating robustness of the amplitude adjustment step. Thus, the leading phase has two-fold advantage: it reduces the peak coil current of the main phase and lowers its activation threshold. Importantly, the threshold orientation maps of the optimized waveforms were scaled versions of the maps for monophasic pulses [46] given the negligible variability (10^{-15}) of the scaling factors across E-field orientations for the individual Blue Brain models, indicating that the directional selectivity has not changed compared to the monophasic pulse.

The best optimized waveforms with the least losses had only about a quarter of the coil heating compared to conventional monophasic pulses and up to 50% less heating than biphasic pulses. Using these optimized monophasic-equivalent pulses, the pulse rate of TMS protocols can therefore be at least quadrupled or doubled with equal power loss and coil heating compared to conventional monophasic and biphasic pulses, respectively. Further increase in pulse rate can be obtained, considering that the MPS-TMS device does not include resistors but recovers pulse energy, as in conventional biphasic stimulators [37]. The higher pulse rate can be achieved with reduced interstimulus or interburst intervals, increased number of pulses per burst, or a combination of both.

4.2. Comparison with other optimization approaches

Waveform optimization approaches have been developed for neural stimulation and the pulse energy is a common optimization target. However, the highly nonlinear neural response has been a challenge that classic optimization methods have difficulties dealing with. Many studies simply evaluate and compare candidate waveforms defined a priori based on heuristics, such as (multiphasic) rectangular, triangular, rising and falling ramp or exponential, Gaussian, and sinusoidal pulse shapes [72–78]. Classic optimization methods, such as gradient decent [79] or calculus of variations and the related principle of least action [80–82], have only been applied to single-or two- compartment neuron and straight axon models. In contrast, metaheuristic methods such as evolutionary algorithm [83–85] and particle swarm optimization (PSO) [36,62,86,87] can not only deal with the nonlinearity of neural response, but also handle complex neuronal structures, multiple stimulation targets, and activation of neural networks. These methods, however, are computationally expensive as they need to evaluate a large population of tens to hundreds of candidate solutions over hundreds to thousands of iterations and are sometimes repeated with tens to hundreds of trials using different random initialization of the candidate solutions for each trial to ensure convergence [83,85,87].

Instead of imposing both the E-field matching and neural activation constraints simultaneously during the optimization, our approach utilized the waveform relationship between TMS coil current and E-field to separate the neural response from the optimization process and therefore reduced the complexity of the problem significantly. The optimization had a short computational runtime as the neural simulations were only run once per parameter combination to obtain the scaling factors for adjusting the waveform amplitudes. A single-CPU computer can easily handle the optimization and simulation using simple neural models. Parallel computing on a cluster was still required to map the thresholds for all 200 E-field orientations of the 15 Blue Brain models within practical runtime, or similarly to find the threshold distribution of a population of 3000 neurons in the motor cortex of a realistic head model [46]. For example, distributing the 200 simulations over 50 CPUs reduced the runtime for the Blue Brain models to approximately 10 minutes (L2/3 PCs) to 2 hours (L4 interneuron, clone 2) for a given combination of parameters. Nevertheless, the computational cost was significantly less compared to metaheuristic methods, which typically take many days to months to complete even on a compute cluster.

Previous TMS waveform optimization efforts minimized coil heating without limiting the pulse shape to any equivalency while simultaneously accounting for neural activation threshold [36,62]. Only constraining the coil voltage, these optimizations based on particle swarm optimization generated waveforms that had a negative leading phase and a main phase of triangular and rectangular biphasic shapes for the current and the E-field, respectively (Figures 4B). With the slightly negative baseline and the short main phase (25 μs, 50 μs, and 100 μs, respectively), these optimized waveforms from previous work had less heating compared to all three types of conventional pulses. However, their stimulation characteristics would resemble that of a half-sine pulse, which is different compared to monophasic pulses in terms of threshold, activation latency, and directional selectivity [8,10,46]. In comparison, the majority of the optimized waveforms in this work achieved similar performance in terms of heating compared to two of the three waveforms of the previous study (blue and red data points in Figures 4A, corresponding to coil voltage constraints of 990 V and 1960 V in [36], respectively), while retaining the characteristics of conventional monophasic pulses.

4.3. Limitations

Our optimization method utilized the time derivate relationship between the TMS coil current and E-field to generate pulses with equivalent neural activation properties compared to an E-field waveform template. Therefore, the performance of the method was determined by the characteristics of the template and could not be generalized. For example, shifting conventional half-sine and biphasic waveforms in ways similar to the shift in the optimized waveforms also reduced coil heating, albeit to a lesser extend (Figures S13 and S14, Panel A and dashed lines in leftmost column of Panel B), and after the threshold-based amplitude adjustment, the reduction in heating of the optimized half-sine and biphasic waveforms was further diminished (Figures S13 and S14, Panels B and C). Whereas a 10%–50% less heating could be achieved for half-sine waveforms, the biphasic waveform, with a close to zero mean for the coil current, the heating was largely unchanged (between −0.1% and −12%) considering adjustment based on the thresholds of the Blue Brain models. Therefore, our approach can be applied to mostly unidirectional current pulses, e.g., monophasic and half-sine pulses, whereas other methods are needed to design energy-efficient waveforms equivalent to other pulse shapes or without equivalency.

5. Conclusion

We developed a two-step waveform optimization method to design TMS pulses with significantly lower coil heating compared to conventional monophasic pulses but with estimated stimulation effects equivalent to the latter. The first optimization step exploited the temporal relationship of the coil current and the induced E-field to generate candidate waveforms without the necessity of performing neural simulations. The final optimized waveforms were obtained by adjusting the amplitude of the candidate waveforms to account for neural activation. The optimized pulses used as little as 25% of the energy of a monophasic pulse. Such aggressive reduction of coil heating and power losses in the device to just a fraction of the previous levels in combination with modern device technology

that can recover pulse energy enables rapid-rate patterned stimulation protocols while maintaining the orientation selectivity and changes in excitability produced by monophasic pulses.

Acknowledgments

This work was supported by Grant No. RF1MH124943 from the National Institute of Mental Health of the National Institutes of Health of the United States of America; the content is solely the responsibility of the authors and does not necessarily represent the official views of the funding agency. Computational support was provided by the Duke Compute Cluster.

Availability statement

The code and data that support the findings of this study are available upon reasonable request from the authors.

Author contribution

S. M. Goetz, A. V. Peterchev, and W. M. Grill conceived, supervised, and obtained funding and computational resources for the study. B. Wang performed the waveform optimization and neuron modeling, data analysis, and visualization. Z. Li and J. Zhang developed the MPS-TMS system and control program. J. Zhang performed the experiment and recorded the optimized waveforms. B. Wang, J. Zhang, and S. M. Goetz wrote the manuscript, and all authors revised, commented on, and approved the final version of the manuscript.

Conflict of interest

S. M. Goetz is inventor on patents and patent applications on MPS TMS, related power electronics circuits, and other TMS technology. Related to TMS technology, S. M. Goetz has previously received royalties from Rogue Research as well as research funding from Magstim; A. V. Peterchev is inventor on patents on TMS technology and has received research funding, travel support, patent royalties, consulting fees, equipment loans, hardware donations, and/or patent application support from Rogue Research, Magstim, MagVenture, Neuronetics, BTL Industries, Advise Connect Inspire, Ampa, and Soterix Medical. B. Wang, Z. Li, J. Zhang, and W. M. Grill declare no relevant conflict of interest.

References

[1] Luan S, Williams I, Nikolic K and Constandinou T G 2014 Neuromodulation: present and emerging methods *Front. Neuroengineering* **7**

[2] Luber B and Lisanby S H 2014 Enhancement of human cognitive performance using transcranial magnetic stimulation (TMS) *NeuroImage* **85** 961–70

[3] Eldaief M C, Press D Z and Pascual-Leone A 2013 Transcranial magnetic stimulation in neurology: A review of established and prospective applications *Neurol. Clin. Pract.* **3** 519–26

[4] Rossi S, Antal A, Bestmann S, Bikson M, Brewer C, Brockmöller J, Carpenter L L, Cincotta M, Chen R, Daskalakis J D, Di Lazzaro V, Fox M D, George M S, Gilbert D, Kimiskidis V K, Koch G, Ilmoniemi R J, Pascal Lefaucheur J, Leocani L, Lisanby S H, Miniussi C, Padberg F, Pascual-Leone A, Paulus W, Peterchev A V, Quartarone A, Rotenberg A, Rothwell J, Rossini P M, Santarnecchi E, Shafi M M, Siebner H R, Ugawa

Y, Wassermann E M, Zangen A, Ziemann U and Hallett M 2020 Safety and recommendations for TMS use in healthy subjects and patient populations, with updates on training, ethical and regulatory issues: Expert Guidelines *Clin. Neurophysiol.*

[5] Wang B, Aberra A S, Grill W M and Peterchev A V 2021 Physics and Biophysics Fundamentals of Transcranial Stimulation *The Oxford Handbook of Transcranial Stimulation* ed E M Wassermann, V Walsh, A V Peterchev, U Ziemann, S Lisanby and H Siebner (Oxford: Oxford University Press) p 23

[6] Goetz S M, Luber B, Lisanby S H, Murphy D L K, Kozyrkov I C, Grill W M and Peterchev A V 2016 Enhancement of Neuromodulation with Novel Pulse Shapes Generated by Controllable Pulse Parameter Transcranial Magnetic Stimulation *Brain Stimulat.* **9** 39–47

[7] Halawa I, Reichert K, Aberra A S, Sommer M, Peterchev A V and Paulus W 2021 Effect of Pulse Duration and Direction on Plasticity Induced by 5 Hz Repetitive Transcranial Magnetic Stimulation in Correlation With Neuronal Depolarization *Front. Neurosci.* **15** 1566

[8] Sommer M, Alfaro A, Rummel M, Speck S, Lang N, Tings T and Paulus W 2006 Half sine, monophasic and biphasic transcranial magnetic stimulation of the human motor cortex *Clin. Neurophysiol.* **117** 838–44

[9] Sommer M, Norden C, Schmack L, Rothkegel H, Lang N and Paulus W 2013 Opposite Optimal Current Flow Directions for Induction of Neuroplasticity and Excitation Threshold in the Human Motor Cortex *Brain Stimulat.* **6** 363–70

[10] Sommer M, Ciocca M, Chieffo R, Hammond P, Neef A, Paulus W, Rothwell J C and Hannah R 2018 TMS of primary motor cortex with a biphasic pulse activates two independent sets of excitable neurones *Brain Stimulat.* **11** 558–65

[11] Arai N, Okabe S, Furubayashi T, Terao Y, Yuasa K and Ugawa Y 2005 Comparison between short train, monophasic and biphasic repetitive transcranial magnetic stimulation (rTMS) of the human motor cortex *Clin. Neurophysiol.* **116** 605–13

[12] Arai N, Okabe S, Furubayashi T, Mochizuki H, Iwata N K, Hanajima R, Terao Y and Ugawa Y 2007 Differences in after-effect between monophasic and biphasic high-frequency rTMS of the human motor cortex *Clin. Neurophysiol.* **118** 2227–33

[13] Hosono Y, Urushihara R, Harada M, Morita N, Murase N, Kunikane Y, Shimazu H, Asanuma K, Uguisu H and Kaji R 2008 Comparison of monophasic versus biphasic stimulation in rTMS over premotor cortex: SEP and SPECT studies *Clin. Neurophysiol.* **119** 2538–45

[14] Taylor J L and Loo C K 2007 Stimulus waveform influences the efficacy of repetitive transcranial magnetic stimulation *J. Affect. Disord.* **97** 271–6

[15] Tings T, Lang N, Tergau F, Paulus W and Sommer M 2005 Orientation-specific fast rTMS maximizes corticospinal inhibition and facilitation *Exp. Brain Res.* **164** 323–33

[16] Barker A T, Jalinous R and Freeston I L 1985 Non-invasive magnetic stimulation of human motor cortex *The Lancet* **325** 1106–1107

[17] Goetz S M, Weyh T, Afinowi I A A and Herzog H G 2014 Coil Design for Neuromuscular Magnetic Stimulation Based on a Detailed 3-D Thigh Model *IEEE Trans. Magn.* **50** 1–10

[18] Jalinous R 1991 Technical and Practical Aspects of Magnetic Nerve Stimulation *J. Clin. Neurophysiol.* **8** 10–25

[19] Peterchev A V, Deng Z-D and Goetz S M 2015 Advances in Transcranial Magnetic Stimulation Technology *Brain Stimulation* ed I M R MBBS (John Wiley & Sons, Inc) pp 165–89

[20] International Electrotechnical Commission 2000 IEC 60601-1-1 Medical Electrical Equipment-Part 1: General Requirements for Safety 1: Collateral Standard: Safety Requirements for Medical Electrical Systems

[21] Goetz S M and Deng Z-D 2017 The development and modelling of devices and paradigms for transcranial magnetic stimulation *Int. Rev. Psychiatry* **29** 115–45

[22] Huang Y-Z and Rothwell J C 2004 The effect of short-duration bursts of high-frequency, low-intensity transcranial magnetic stimulation on the human motor cortex *Clin. Neurophysiol.* **115** 1069–75

[23] Matsumoto H and Ugawa Y 2020 Quadripulse stimulation (QPS) *Exp. Brain Res.* **238** 1619–25

[24] Di Lazzaro V, Dileone M, Pilato F, Capone F, Musumeci G, Ranieri F, Ricci V, Bria P, Di Iorio R, de Waure C, Pasqualetti P and Profice P 2011 Modulation of motor cortex neuronal networks by rTMS: comparison of local and remote effects of six different protocols of stimulation *J. Neurophysiol.* **105** 2150–6

[25] Nakamura K, Groiss S J, Hamada M, Enomoto H, Kadowaki S, Abe M, Murakami T, Wiratman W, Chang F, Kobayashi S, Hanajima R, Terao Y and Ugawa Y 2016 Variability in Response to Quadripulse Stimulation of the Motor Cortex *Brain Stimulat.* **9** 859–66

[26] Simeoni S, Hannah R, Sato D, Kawakami M, Rothwell J, Simeoni S, Gigli G L, Sato D and Kawakami M 2016 Effects of Quadripulse Stimulation on Human Motor Cortex Excitability: A Replication Study *Brain Stimul. Basic Transl. Clin. Res. Neuromodulation* **9** 148–50

[27] Hamada M, Hanajima R, Terao Y, Arai N, Furubayashi T, Inomata-Terada S, Yugeta A, Matsumoto H, Shirota Y and Ugawa Y 2007 Quadro-pulse stimulation is more effective than paired-pulse stimulation for plasticity induction of the human motor cortex *Clin. Neurophysiol.* **118** 2672–82

[28] Tiksnadi A, Murakami T, Wiratman W and Ugawa Y 2019 Higher Efficacy and Less Inter-individual Variability in QPS than TBS: Head to Head Comparison Study *Brain Stimulat.* **12** 434

[29] Hamada M, Terao Y, Hanajima R, Shirota Y, Nakatani-Enomoto S, Furubayashi T, Matsumoto H and Ugawa Y 2008 Bidirectional long-term motor cortical plasticity and metaplasticity induced by quadripulse transcranial magnetic stimulation *J. Physiol.* **586** 3927–47

[30] Hamada M and Ugawa Y 2010 Quadripulse stimulation – A new patterned rTMS *Restor. Neurol. Neurosci.* **28** 7

[31] Jung N H, Gleich B, Kalb A, Limburg K, Gattinger N, Fritsch J, Siebner H R and Mall V 2015 P145. Transcranial biphasic quadro-pulse stimulation with one but not two full-sine cycles induces long-term depression-like corticomotor plasticity *Clin. Neurophysiol.* **126** e134

[32] Jung N H, Gleich B, Gattinger N, Hoess C, Haug C, Siebner H R and Mall V 2016 Quadri-Pulse Theta Burst Stimulation using Ultra-High Frequency Bursts – A New Protocol to Induce Changes in Cortico-Spinal Excitability in Human Motor Cortex *PLOS ONE* **11** e0168410

[33] Levkovitz Y, Isserles M, Padberg F, Lisanby S H, Bystritsky A, Xia G, Tendler A, Daskalakis Z J, Winston J L, Dannon P, Hafez H M, Reti I M, Morales O G, Schlaepfer T E, Hollander E, Berman J A, Husain M M, Sofer U, Stein A, Adler S, Deutsch L, Deutsch F, Roth Y, George M S and Zangen A 2015 Efficacy and safety of deep transcranial magnetic stimulation for major depression: a prospective multicenter randomized controlled trial *World Psychiatry* **14** 64–73

[34] Blumberger D M, Vila-Rodriguez F, Thorpe K E, Feffer K, Noda Y, Giacobbe P, Knyahnytska Y, Kennedy S H, Lam R W, Daskalakis Z J and Downar J 2018 Effectiveness of theta burst versus high-frequency repetitive transcranial magnetic stimulation in patients with depression (THREE-D): a randomised non-inferiority trial *The Lancet* **391** 1683–92

[35] O'Reardon J P, Solvason H B, Janicak P G, Sampson S, Isenberg K E, Nahas Z, McDonald W M, Avery D, Fitzgerald P B, Loo C, Demitrack M A, George M S and Sackeim H A 2007 Efficacy and Safety of Transcranial Magnetic Stimulation in the Acute Treatment of Major Depression: A Multisite Randomized Controlled Trial *Biol. Psychiatry* **62** 1208–16

[36] Goetz S M, Truong C N, Gerhofer M G, Peterchev A V, Herzog H-G and Weyh T 2013 Analysis and Optimization of Pulse Dynamics for Magnetic Stimulation *PLOS ONE* **8** e55771

[37] Goetz S M, Pfaeffl M, Huber J, Singer M, Marquardt R and Weyh T 2012 Circuit topology and control principle for a first magnetic stimulator with fully controllable waveform *2012 Annual International Conference of the IEEE Engineering in Medicine and Biology Society* 2012 Annual International Conference of the IEEE Engineering in Medicine and Biology Society pp 4700–3

[38] Goetz S M, Singer M, Huber J, Pfaeffl M, Marquardt R and Weyh T 2013 Magnetic Stimulation with Arbitrary Waveform Shapes *World Congress on Medical Physics and Biomedical Engineering May 26-31, 2012, Beijing, China* (Springer) pp 2244–2247

[39] Goetz S M, Peterchev A V and Weyh T 2015 Modular Multilevel Converter With Series and Parallel Module Connectivity: Topology and Control *IEEE Trans. Power Electron.* **30** 203–15

[40] Li Z, Zhang J, Peterchev A V and Goetz S M 2022 Modular Pulse Synthesizer for Transcranial Magnetic Stimulation with Flexible User-Defined Pulse Shaping and Rapidly Changing Pulses in Sequences *ArXiv220206530 Phys.*

[41] Neukirchinger F, Kersten A, Kuder M, Lohse B, Schwitzgebel F and Weyh T 2021 Where Transcranial Magnetic Stimulation is headed to: The Modular Extended Magnetic Stimulator *2021 IEEE International*

Conference on Environment and Electrical Engineering and 2021 IEEE Industrial and Commercial Power Systems Europe (EEEIC / I&CPS Europe) 2021 IEEE International Conference on Environment and Electrical Engineering and 2021 IEEE Industrial and Commercial Power Systems Europe (EEEIC / I&CPS Europe) (Bari, Italy: IEEE) pp 1–6

[42] Zeng Z, Koponen L M, Hamdan R, Li Z, Goetz S M and Peterchev A V 2022 Modular multilevel TMS device with wide output range and ultrabrief pulse capability for sound reduction *J. Neural Eng.* **19** 026008

[43] D'Ostilio K, Goetz S M, Hannah R, Ciocca M, Chieffo R, Chen J-C A, Peterchev A V and Rothwell J C 2016 Effect of coil orientation on strength–duration time constant and I-wave activation with controllable pulse parameter transcranial magnetic stimulation *Clin. Neurophysiol.* **127** 675–83

[44] Sorkhabi M M, Wendt K, O'Shea J and Denison T 2022 Pulse width modulation-based TMS: Primary motor cortex responses compared to conventional monophasic stimuli *Brain Stimul. Basic Transl. Clin. Res. Neuromodulation* **15** 980–3

[45] Peterchev A V and Riehl M E 2022 Transcranial Magnetic Stimulators *The Oxford Handbook of TMS* ed E M Wassermann, V Walsh, A V Peterchev, U Ziemann, S Lisanby and H Siebner (Oxford: Oxford University Press)

[46] Aberra A S, Wang B, Grill W M and Peterchev A V 2020 Simulation of transcranial magnetic stimulation in head model with morphologically-realistic cortical neurons *Brain Stimulat.* **13** 175–89

[47] Barker A T, Garnham C W and Freeston I L 1991 Magnetic nerve stimulation: the effect of waveform on efficiency, determination of neural membrane time constants and the measurement of stimulator output *Electroencephalogr. Clin. Neurophysiol. Suppl.* **43** 227–37

[48] Peterchev A V, Goetz S M, Westin G G, Luber B and Lisanby S H 2013 Pulse width dependence of motor threshold and input–output curve characterized with controllable pulse parameter transcranial magnetic stimulation *Clin. Neurophysiol.* **124** 1364–72

[49] McIntyre C C, Richardson A G and Grill W M 2002 Modeling the Excitability of Mammalian Nerve Fibers: Influence of Afterpotentials on the Recovery Cycle *J. Neurophysiol.* **87** 995–1006

[50] Mainen Z F, Joerges J, Huguenard J R and Sejnowski T J 1995 A model of spike initiation in neocortical pyramidal neurons *Neuron* **15** 1427–39

[51] Mainen Z F and Sejnowski T J 1996 Influence of dendritic structure on firing pattern in model neocortical neurons *Nature* **382** 363–6

[52] Markram H, Muller E, Ramaswamy S, Reimann M W, Abdellah M, Sanchez C A, Ailamaki A, Alonso-Nanclares L, Antille N, Arsever S, Kahou G A A, Berger T K, Bilgili A, Buncic N, Chalimourda A, Chindemi G, Courcol J-D, Delalondre F, Delattre V, Druckmann S, Dumusc R, Dynes J, Eilemann S, Gal E, Gevaert M E, Ghobril J-P, Gidon A, Graham J W, Gupta A, Haenel V, Hay E, Heinis T, Hernando J B, Hines M, Kanari L, Keller D, Kenyon J, Khazen G, Kim Y, King J G, Kisvarday Z, Kumbhar P, Lasserre S, Le Bé J-V, Magalhães B R C, Merchán-Pérez A, Meystre J, Morrice B R, Muller J, Muñoz-Céspedes A, Muralidhar S, Muthurasa K, Nachbaur D, Newton T H, Nolte M, Ovcharenko A, Palacios J, Pastor L, Perin R, Ranjan R, Riachi I, Rodríguez J-R, Riquelme J L, Rössert C, Sfyrakis K, Shi Y, Shillcock J C, Silberberg G, Silva R, Tauheed F, Telefont M, Toledo-Rodriguez M, Tränkler T, Van Geit W, Díaz J V, Walker R, Wang Y, Zaninetta S M, DeFelipe J, Hill S L, Segev I and Schürmann F 2015 Reconstruction and Simulation of Neocortical Microcircuitry *Cell* **163** 456–92

[53] Aberra A S, Peterchev A V and Grill W M 2018 Biophysically Realistic Neuron Models for Simulation of Cortical Stimulation *J. Neural Eng.* **15** 066023

[54] Hines M L and Carnevale N T 1997 The NEURON Simulation Environment *Neural Comput.* **9** 1179–209

[55] Bikson M, Dmochowski J and Rahman A 2013 The "Quasi-Uniform" Assumption in Animal and Computational Models of Non-Invasive Electrical Stimulation *Brain Stimulat.* **6** 704–5

[56] Wang B, Aberra A S, Grill W M and Peterchev A V 2022 Responses of Model Cortical Neurons to Temporal Interference Stimulation and Other Transcranial Alternating Current Stimulation Modalities *bioRxiv* 2022.05.04.490540

[57] Koponen L M, Nieminen J O, Mutanen T P, Stenroos M and Ilmoniemi R J 2017 Coil optimisation for transcranial magnetic stimulation in realistic head geometry *Brain Stimulat.* **10** 795–805

[58] Koponen L M, Goetz S M, Tucci D L and Peterchev A V 2020 Sound comparison of seven TMS coils at matched stimulation strength *Brain Stimulat.* **13** 873–80
[59] Nieminen J O, Koponen L M and Ilmoniemi R J 2015 Experimental Characterization of the Electric Field Distribution Induced by TMS Devices *Brain Stimulat.* **8** 582–9
[60] Kammer T, Beck S, Thielscher A, Laubis-Herrmann U and Topka H 2001 Motor thresholds in humans: a transcranial magnetic stimulation study comparing different pulse waveforms, current directions and stimulator types *Clin. Neurophysiol.* **112** 250–8
[61] Kammer T, Vorwerg M and Herrnberger B 2007 Anisotropy in the visual cortex investigated by neuronavigated transcranial magnetic stimulation *NeuroImage* **36** 313–21
[62] Goetz S M, Truong N C, Gerhofer M G, Peterchev A V, Herzog H and Weyh T 2012 Optimization of magnetic neurostimulation waveforms for minimum power loss *2012 Annual International Conference of the IEEE Engineering in Medicine and Biology Society (EMBC)* 2012 Annual International Conference of the IEEE Engineering in Medicine and Biology Society (EMBC) pp 4652–5
[63] Zacharias L R, Peres A S C, Souza V H, Conforto A B and Baffa O 2019 Method to assess the mismatch between the measured and nominal parameters of transcranial magnetic stimulation devices *J. Neurosci. Methods* **322** 83–7
[64] Peterchev A V, Jalinous R and Lisanby S H 2008 A Transcranial Magnetic Stimulator Inducing Near-Rectangular Pulses With Controllable Pulse Width (cTMS) *IEEE Trans. Biomed. Eng.* **55** 257–66
[65] Peterchev A V, Murphy D L and Lisanby S H 2011 Repetitive transcranial magnetic stimulator with controllable pulse parameters *J. Neural Eng.* **8** 036016
[66] Shirinpour S, Alekseichuk I, Mantell K and Opitz A 2020 Experimental evaluation of methods for real-time EEG phase-specific transcranial magnetic stimulation *J. Neural Eng.* **17** 046002
[67] Eickhoff S and Jarvis J C 2020 The effect of sub-threshold pre-pulses on neural activation depends on electrode configuration *IEEE Trans. Biomed. Eng.* **67** 2552–2559
[68] Ghobreal B, Nadim F and Sahin M 2022 Selective neural stimulation by leveraging electrophysiological differentiation and using pre-pulsing and non-rectangular waveforms *J. Comput. Neurosci.*
[69] Grill W M 2018 Chapter 8 - Waveforms for Neural Stimulation *Neuromodulation: Comprehensive Textbook of Principles, Technologies, and Therapies* vol 1, ed E S Krames, P H Peckham and A R Rezai (Academic Press) pp 95–102
[70] Grill W M and Mortimer J T 1995 Stimulus waveforms for selective neural stimulation *IEEE Eng. Med. Biol. Mag.* **14** 375–85
[71] Smit J E, Hanekom T, van Wieringen A, Wouters J and Hanekom J J 2010 Threshold predictions of different pulse shapes using a human auditory nerve fibre model containing persistent sodium and slow potassium currents *Hear. Res.* **269** 12–22
[72] Eickhoff S and Jarvis J C 2020 An Investigation of Neural Stimulation Efficiency With Gaussian Waveforms *IEEE Trans. Neural Syst. Rehabil. Eng.* **28** 104–12
[73] Foutz T J, Jr D M A, Kilgore K L and McIntyre C C 2012 Energy Efficient Neural Stimulation: Coupling Circuit Design and Membrane Biophysics *PLOS ONE* **7** e51901
[74] Foutz T J and McIntyre C C 2010 Evaluation of novel stimulus waveforms for deep brain stimulation *J. Neural Eng.* **7** 066008
[75] Lee J-I and Im M 2018 Non-rectangular waveforms are more charge-efficient than rectangular one in eliciting network-mediated responses of ON type retinal ganglion cells *J. Neural Eng.* **15** 055004
[76] Rapp J, Braun P, Hemmert W and Gleich B 2022 Optimal pulse configuration for peripheral inductive nerve stimulation *Biomed. Phys. Eng. Express*
[77] Sahin M and Tie Y 2007 Non-rectangular waveforms for neural stimulation with practical electrodes *J. Neural Eng.* **4** 227–33
[78] Wongsarnpigoon A, Woock J P and Grill W M 2010 Efficiency Analysis of Waveform Shape for Electrical Excitation of Nerve Fibers *IEEE Trans. Neural Syst. Rehabil. Eng.* **18** 319–28
[79] Tahayori B and Dokos S 2012 Optimal stimulus current waveshape for a hodgkin-huxley model neuron *Engineering in Medicine and Biology Society (EMBC), 2012 Annual International Conference of the IEEE*

IEEE EMBS 34th Annual International Conference of the IEEE Engineering in Medicine and Biology Society (EMBC), 2012 (San Diego, CA, USA: IEEE) pp 4627–30

[80] Krouchev N I, Danner S M, Vinet A, Rattay F and Sawan M 2014 Energy-Optimal Electrical-Stimulation Pulses Shaped by the Least-Action Principle *PLOS ONE* **9** e90480

[81] Forger D B, Paydarfar D and Clay J R 2011 Optimal Stimulus Shapes for Neuronal Excitation *PLOS Comput. Biol.* **7** e1002089

[82] Yi G-S, Wang J, Li H-Y, Wei X-L and Deng B 2016 Minimum energy control for a two-compartment neuron to extracellular electric fields *Commun. Nonlinear Sci. Numer. Simul.* **40** 138–50

[83] Wongsarnpigoon A and Grill W M 2010 Energy-efficient waveform shapes for neural stimulation revealed with a genetic algorithm *J. Neural Eng.* **7** 046009

[84] Yip M, Bowers P, Noel V, Chandrakasan A and Stankovic K M 2017 Energy-efficient waveform for electrical stimulation of the cochlear nerve *Sci. Rep.* **7** 13582

[85] Cassar I R, Titus N D and Grill W M 2017 An improved genetic algorithm for designing optimal temporal patterns of neural stimulation *J. Neural Eng.* **14** 066013

[86] Chen Y, Wang J, Wei X, Deng B and Che Y 2011 Particle swarm optimization of periodic deep brain stimulation waveforms *Proceedings of the 30th Chinese Control Conference* Proceedings of the 30th Chinese Control Conference pp 754–7

[87] Yi G and Grill W M 2020 Kilohertz waveforms optimized to produce closed-state Na+ channel inactivation eliminate onset response in nerve conduction block *PLOS Comput. Biol.* **16** e1007766

[88] Gomez L J, Dannhauer M, Koponen L M and Peterchev A V 2020 Conditions for numerically accurate TMS electric field simulation *Brain Stimulat.* **13** 157–66

[89] Wang B, Grill W M and Peterchev A V 2018 Coupling Magnetically Induced Electric Fields to Neurons: Longitudinal and Transverse Activation *Biophys. J.* **115** 95–107

Supplement

Contents:

- Additional discussion on relationship between TMS waveforms
- Figures S1–S14

Additional discussion on the relationship between TMS waveforms

Mathematically, the current I_{coil} driving the TMS coil generates a magnetic field $\boldsymbol{B}$ that can be described by the Biot-Savart law under the quasi-static assumption

$$\boldsymbol{B}(\boldsymbol{r},t) = B(t,r)\cdot\hat{\boldsymbol{n}}_B(\boldsymbol{r}) = \frac{\mu_0}{4\pi}\oint_{\mathcal{L}}\frac{I_{\mathrm{coil}}(t)\mathrm{d}\boldsymbol{l}\times\boldsymbol{r}'}{|\boldsymbol{r}'|^3} \quad .$$

Here, μ_0 is the permeability of free space, $\mathrm{d}\boldsymbol{l}$ is the line element along the path $\mathcal{L}$ of the coil windings, $\boldsymbol{r}'$ is the vector from the line element to the point of interest $\boldsymbol{r}$ in space, $\hat{\boldsymbol{n}}_B$ is a unit vector aligned with the magnetic field, and B is the temporal waveform of the magnetic field. This equation assumes that the variation of the current within the windings is negligible or the coil has thin windings compared to the physical dimension of the coil and head. Using volumetric coil current density and volume integral generates more accurate field calculation in the head [88], but does not change the proportionality between the magnetic field and coil current

$$B \propto I_{\mathrm{coil}} \quad .$$

The electromagnetic induction generates an E-field $\boldsymbol{E}$ that contains both the divergence-free primary E-field $\boldsymbol{E}' = -\partial\boldsymbol{A}/\partial t$, where $\boldsymbol{A}$ is the magnetic vector potential that is related to the magnetic field by $\nabla\times\boldsymbol{A} = \boldsymbol{B}$, and the conservative secondary E-field $\boldsymbol{E}''$ due to surface charges on the scalp and tissue boundaries, which accumulate on sub-nanosecond time scales. Therefore, on time scales for neural stimulation (≥1 μs), both E-field components vary with the same temporal waveform and the waveform E of the total E-field is proportional to the time-derivative of the magnetic field

$$E \propto \frac{\mathrm{d}B}{\mathrm{d}t} \quad ,$$

where $\boldsymbol{E} = E\cdot\hat{\boldsymbol{n}}_E$ with $\hat{\boldsymbol{n}}_E$ being the unit vector aligned with the E-field.

The equivalent stimulation currents I_{stim} induced in neuronal compartments are proportional to the local E-field amplitude or its spatial derivative [89]. Therefore considering the temporal domain, neural stimulation is proportional to the time derivative of I_{coil} and directly proportional to the coil voltage

$$I_{\mathrm{stim}} \propto E \propto \frac{\mathrm{d}B}{\mathrm{d}t} \propto \frac{\mathrm{d}I_{\mathrm{coil}}}{\mathrm{d}t} \propto V_{\mathrm{coil}} \quad .$$

Here, the ohmic voltage drop on the coil is assumed to be negligible compared to the inductive voltage, so that

$$V_{\mathrm{coil}} = L_{\mathrm{coil}}\frac{\mathrm{d}I_{\mathrm{coil}}}{\mathrm{d}t} + R_{\mathrm{coil}}I_{\mathrm{coil}} \approx L_{\mathrm{coil}}\frac{\mathrm{d}I_{\mathrm{coil}}}{\mathrm{d}t} \quad ,$$

where R_{coil} and L_{coil} are the coil's resistance and inductance, respectively.

Supplementary figures

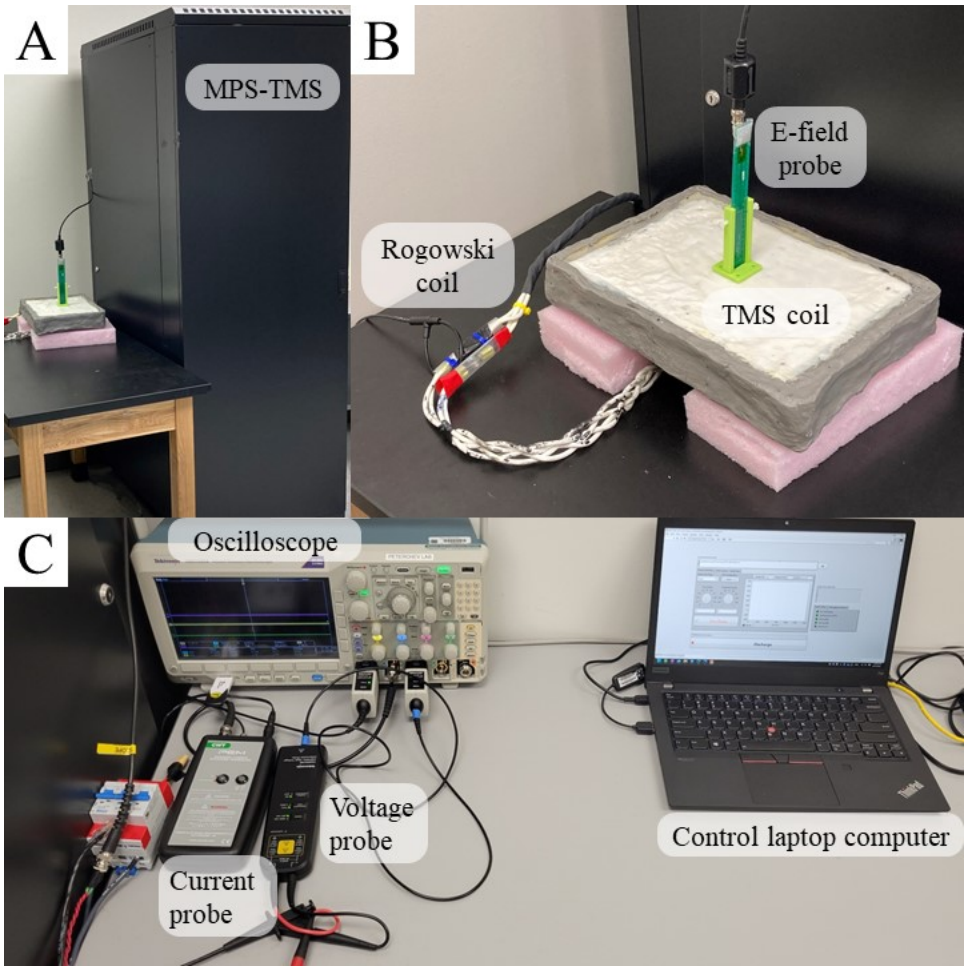

Figure S1: Experimental setup for generating and recording optimized TMS pulses
A. The MPS-TMS system with the custom figure-of-8 coil and E-field measurement setup. **B.** Details of TMS coil with the Rogowski coil attached to the braided coil cable and the PCB-based triangular E-field probe. **C.** The laptop computer running the LabVIEW control program, and the recording setup, with the oscilloscope, Rogowski current transducer, and high-voltage differential probes.

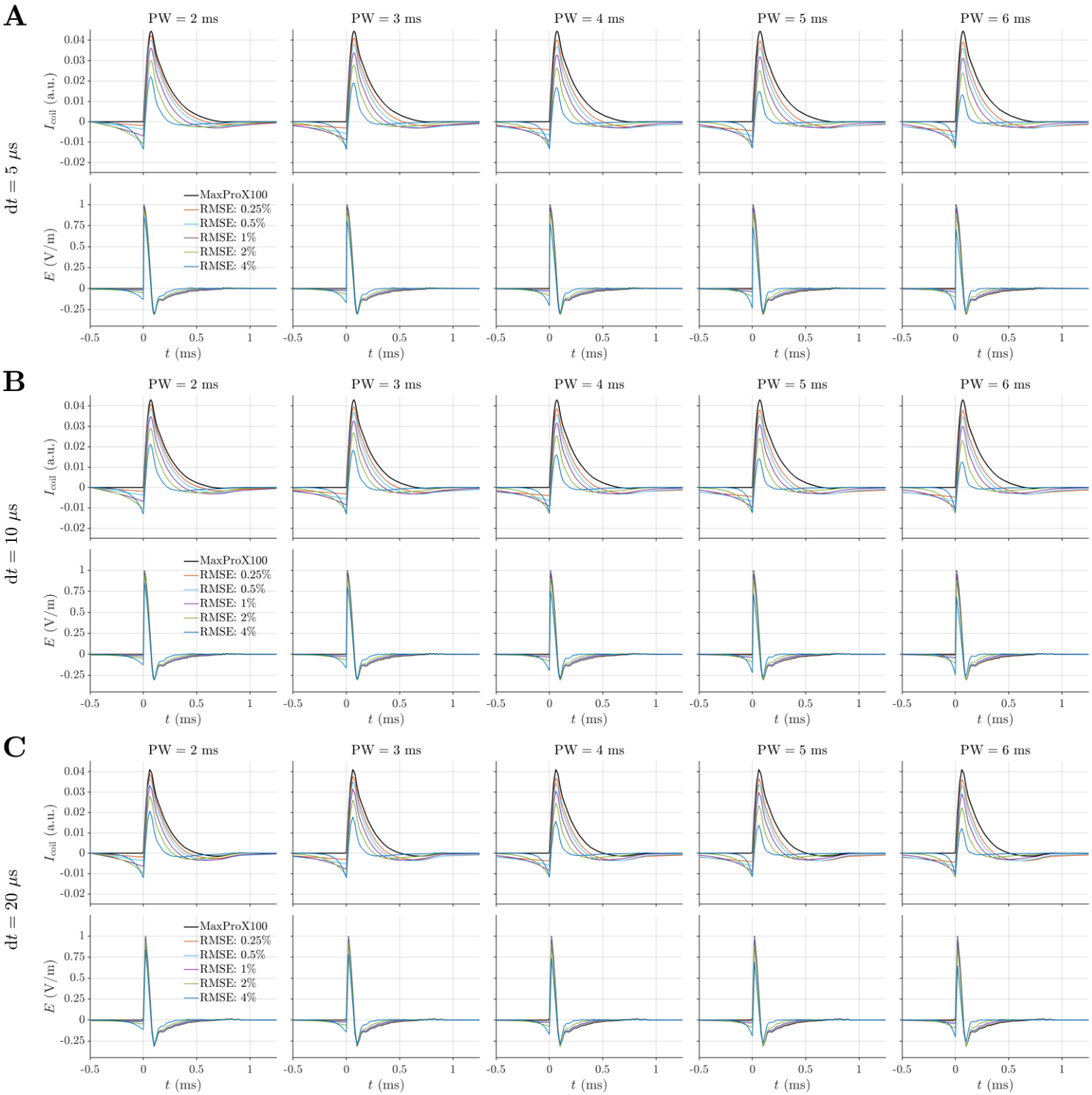

Figure S2: Waveform optimization with different time steps

Similar as Figure 2A, with results for all optimization constraints and for **A** 5 µs, **B** 10 µs, and **C** 20 µs time steps, respectively. Besides the difference in waveform smoothness for the different optimization time steps, the coil currents have slight amplitude difference due to the numerical accuracy of the integration.

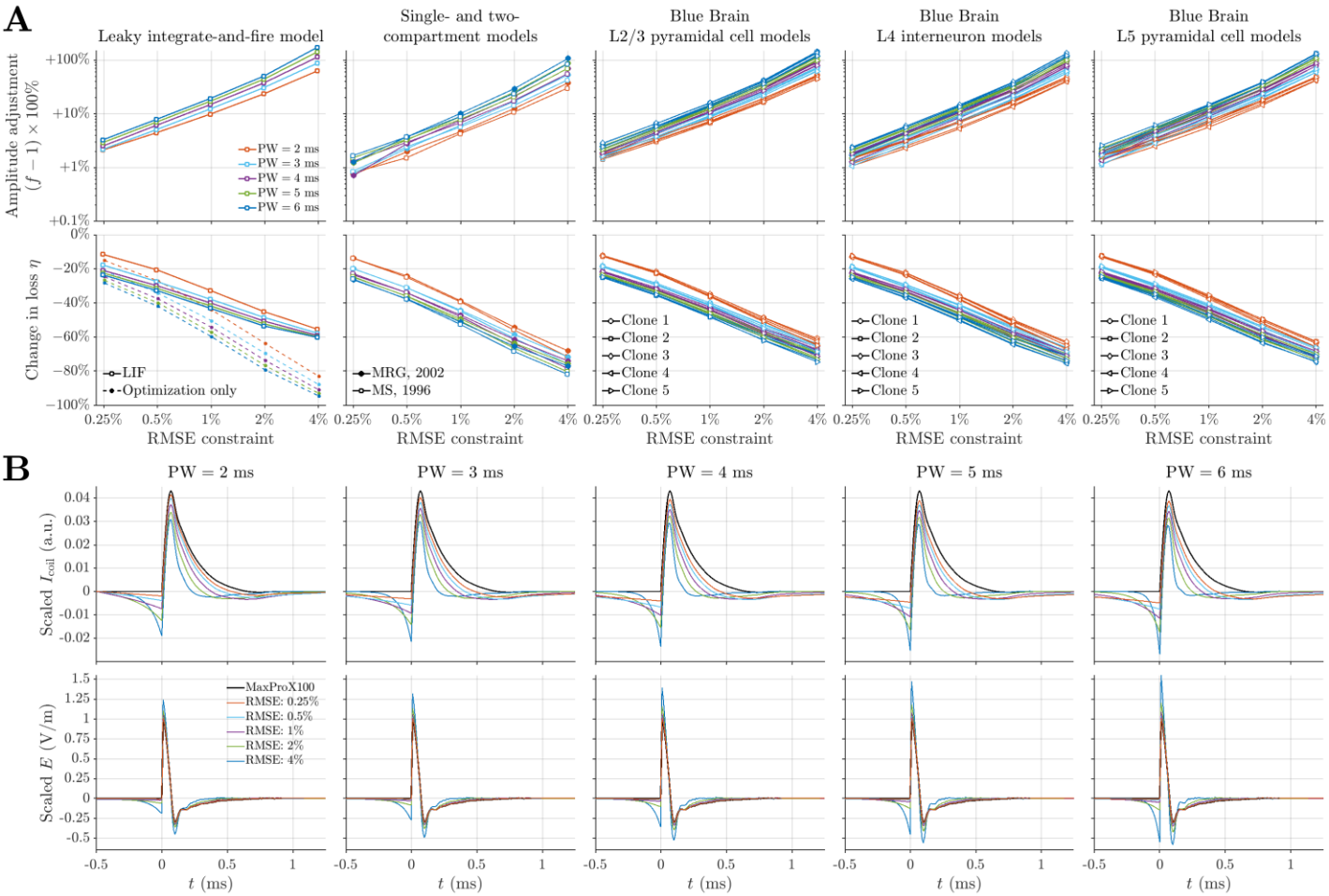

Figure S3: Amplitude adjustment and optimized waveforms for monophasic pulses

Similar as Figure 2, with results for all optimization constraints. **A.** Amplitude adjustment (logarithmic scale) for optimized waveforms to reach threshold for activation for different total pulse durations as a function of the optimization constraints of the E-field. Changes in coil heating compared to the original TMS pulse. **B.** The optimized coil current waveforms and corresponding E-field waveforms (colored lines) after the amplitude adjustment. The original TMS monophasic pulse (black lines) are shown for comparison.

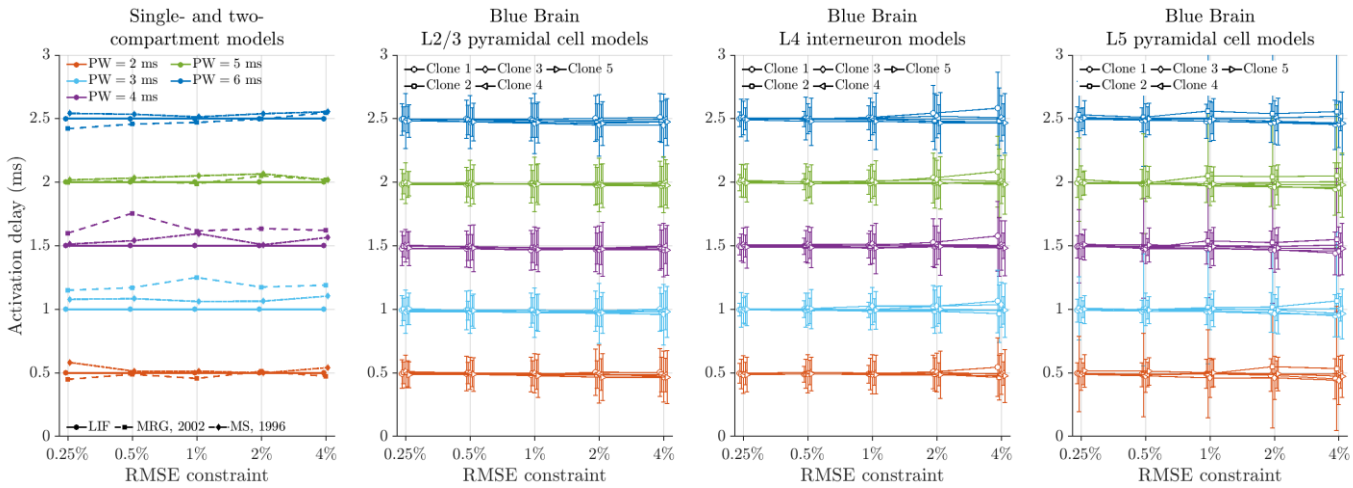

Figure S4: Delay of neural activation

The delay of the action potentials generated by optimized pulses compared to the monophasic pulse. Errors bars show mean and standard deviation of 200 E-field orientations for the Blue Brain models.

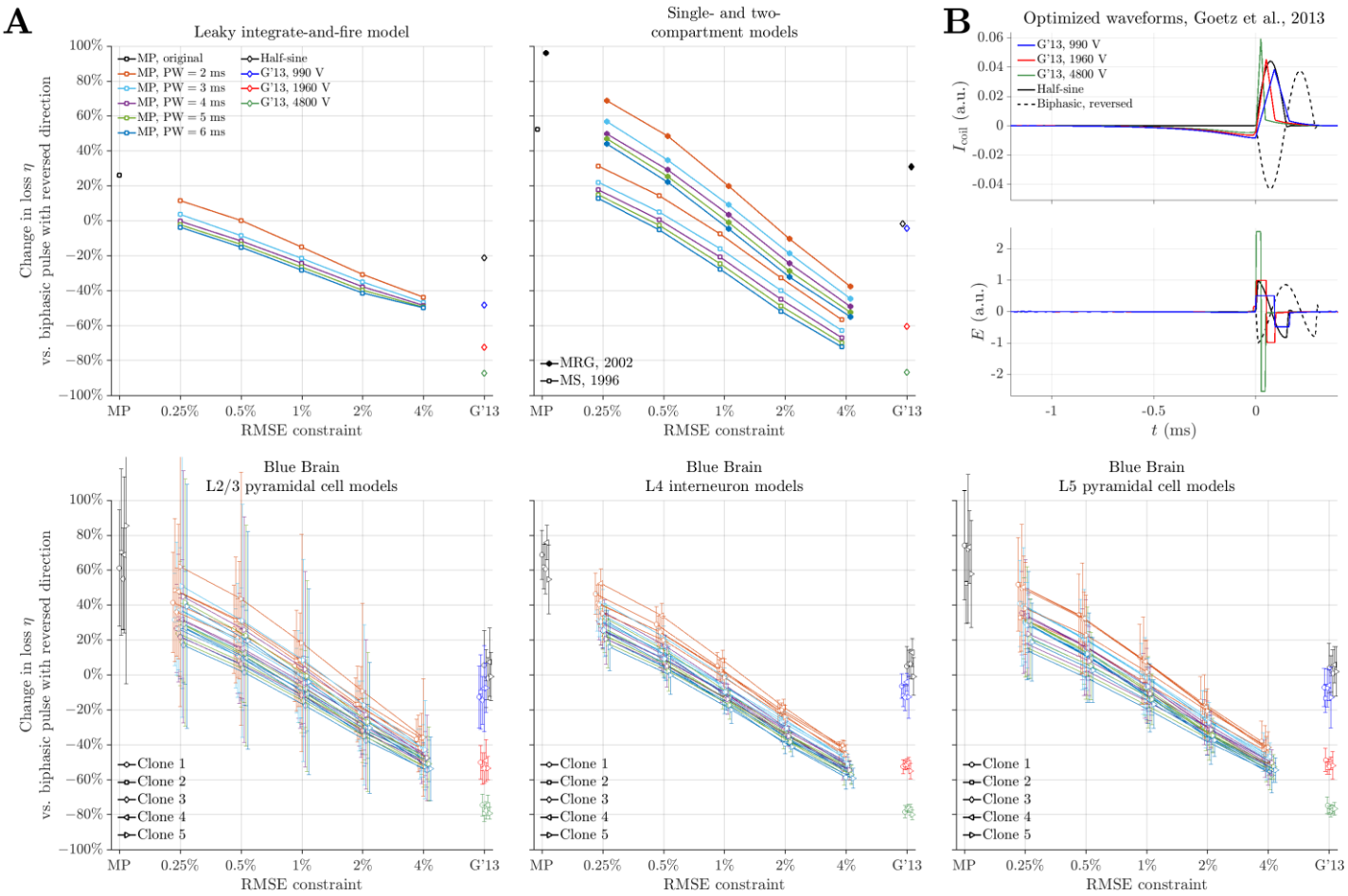

Figure S5: Difference in coil heating comparing monophasic-like pulses and optimized waveforms from a previous study against biphasic pulse

Similar as Figure 4, with results for all pulse durations and Blue Brain model clones in panel A and the full waveform shown for the optimized waveforms from previous work in panel B.

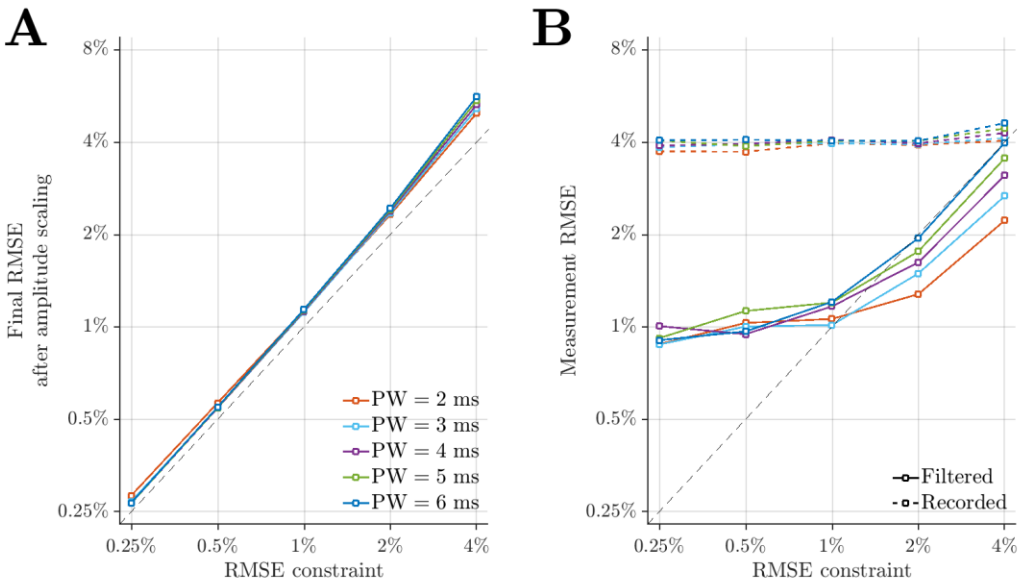

Figure S6: RMSE of computed and measured optimized waveforms

RMSE of the optimized waveform versus the original TMS waveform for computed results (**A)** and recorded waveforms (**B**). The amplitude adjustment step increased the RMSE of the optimized waveforms compared to the RMSE constraint in the first optimization step. The RMSE of the recorded waveforms are subject to noise for the recording for the unfiltered waveforms and around 4% for any optimization parameter whereas the filtered waveform and had either larger or smaller RMSE compared to the RMSE constraint due to the distortion of the filtering process.

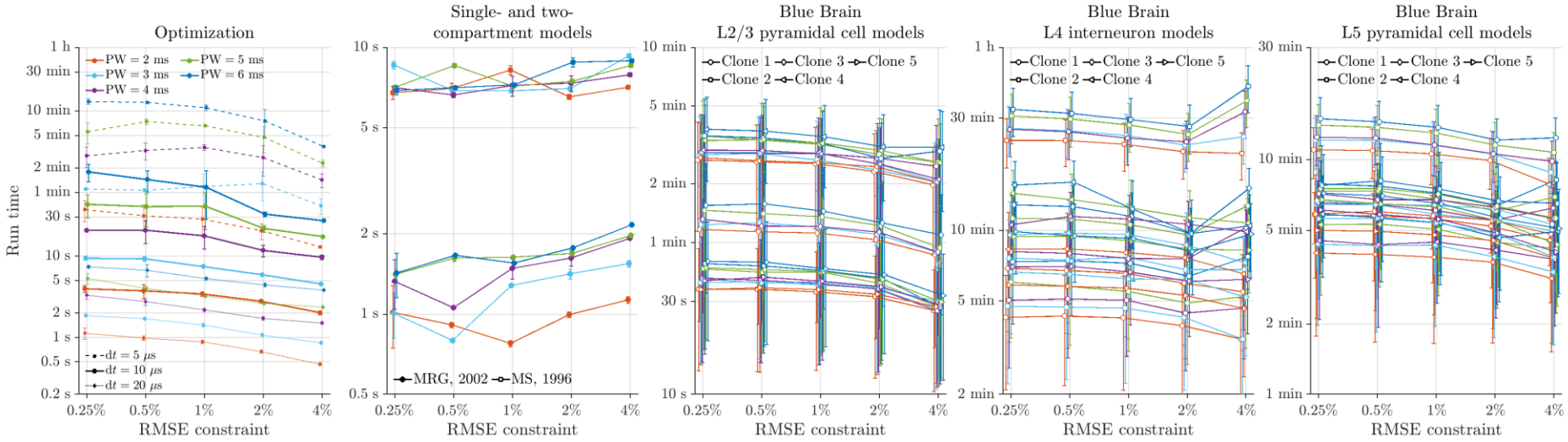

Figure S7: Runtime of optimization and neural simulations

Similar as Figure 5, with results for all pulse durations and Blue Brain model clones.

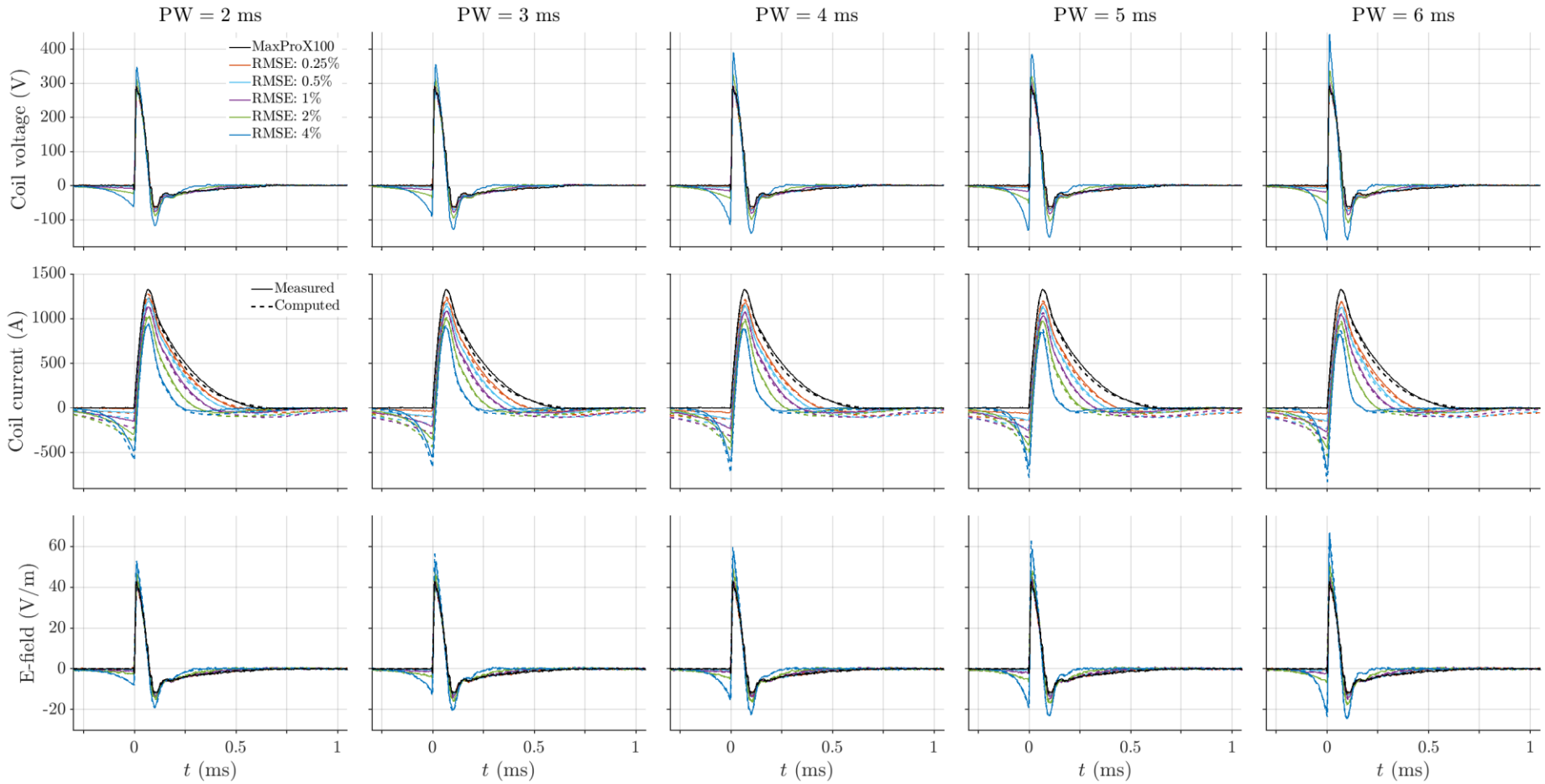

Figure S8: Computed and measured optimized TMS waveforms

Similar as Figure 3, with results for all RMSE and pulse duration constraints.

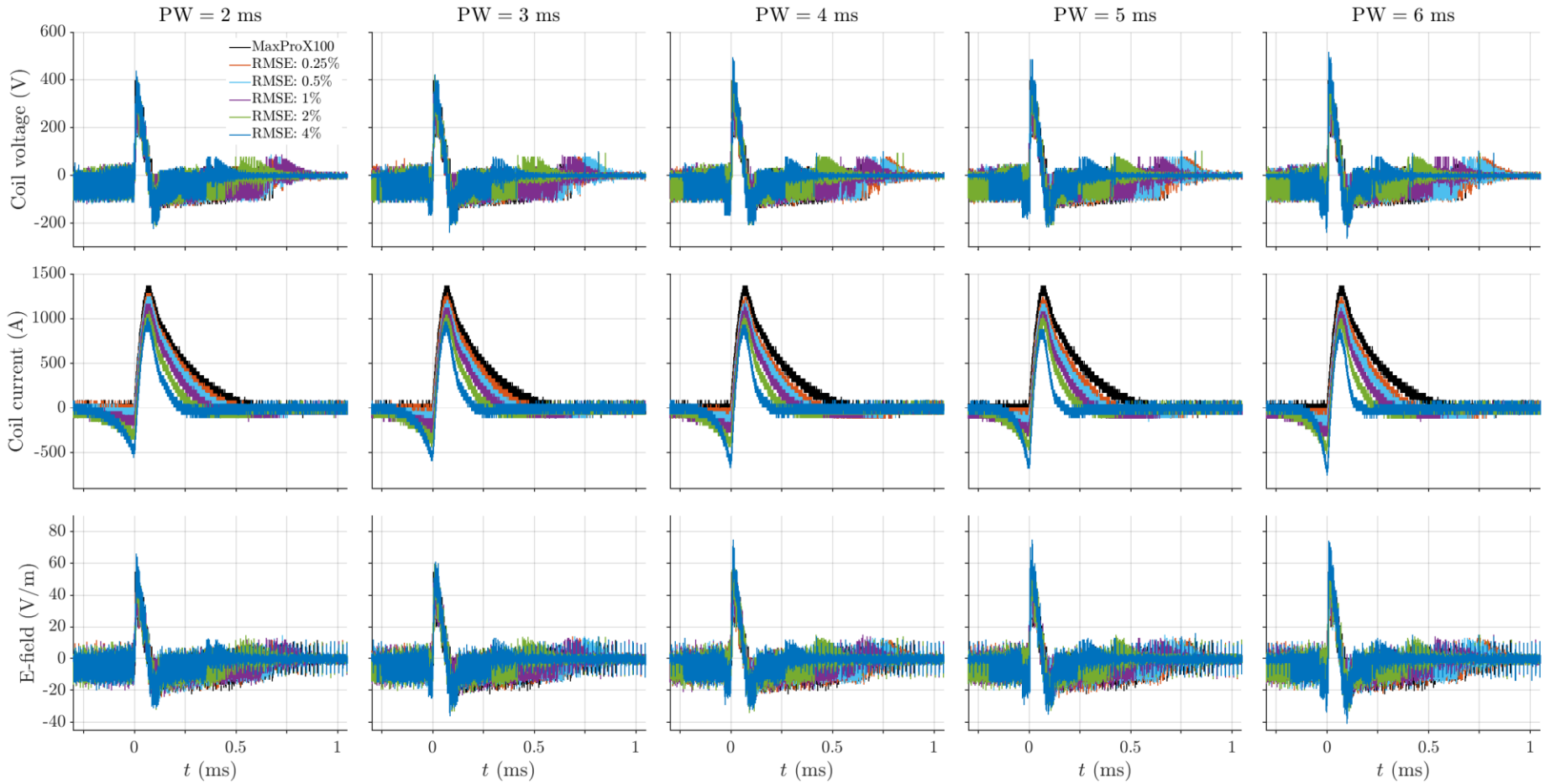

Figure S9: Measured optimized TMS waveforms

Similar as Figure S8, with unfiltered measurements and without the computed waveforms.

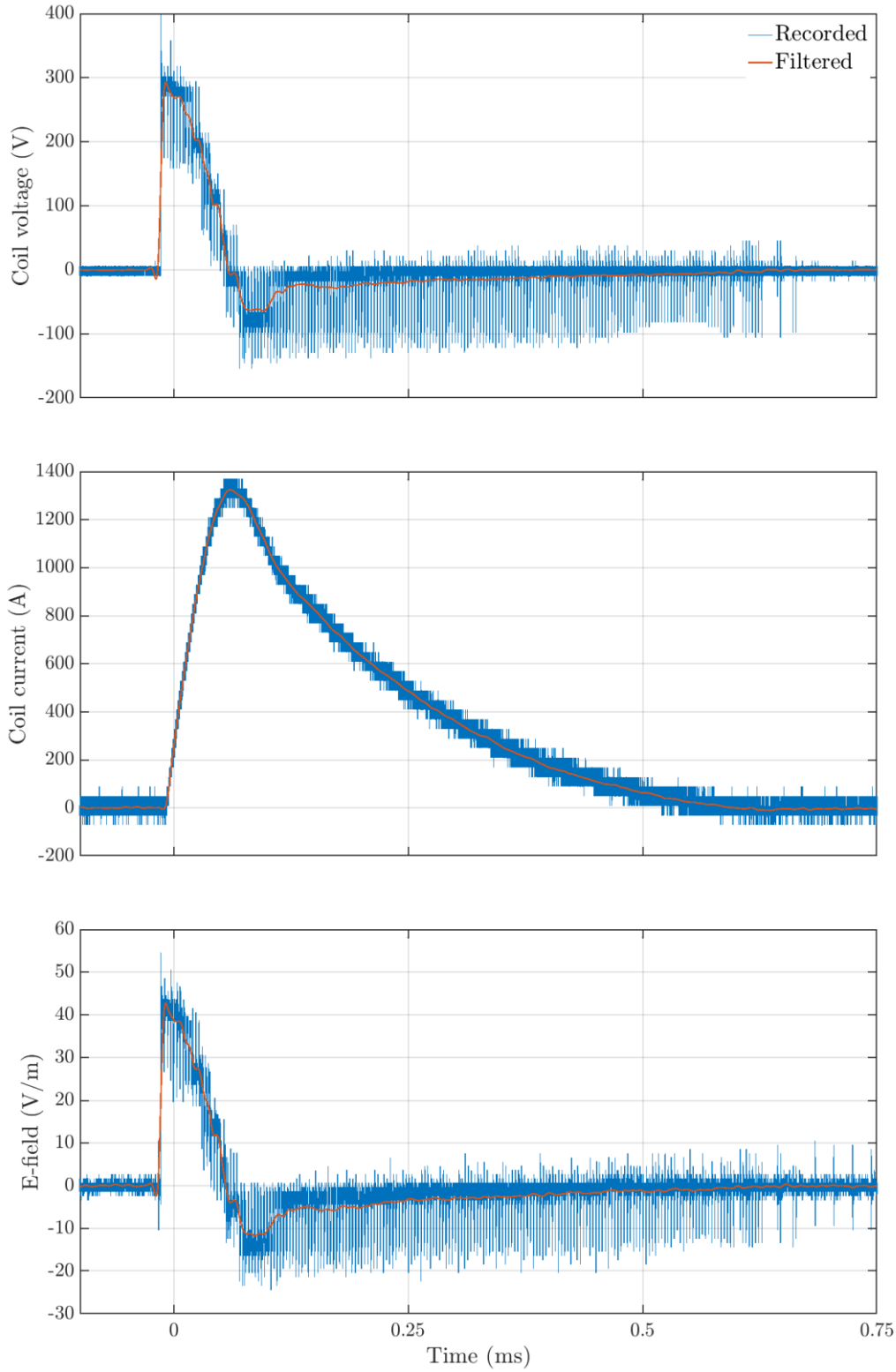

Figure S10: Raw and filtered recordings of the MaxProX100 TMS pulse implemented by MPS-TMS
The coil current only contains high-frequency noise, whereas the coil voltage and E-field waveforms also contain switching noise. Filtering removes most of the noise, but the voltage levels of the modular waveform synthesis is still visible.

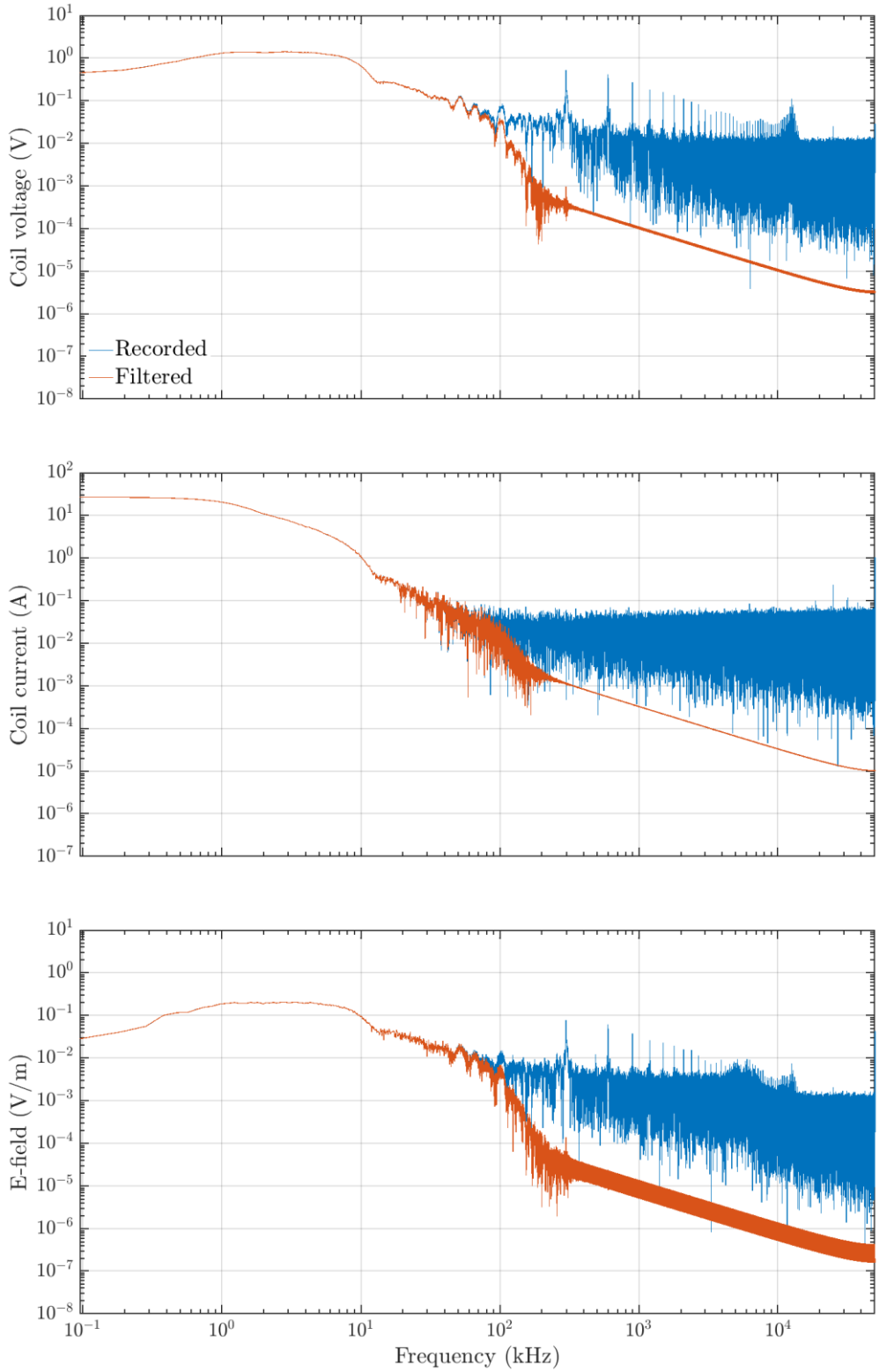

Figure S11: Spectra of raw and filtered recordings of the MPS-TMS-implemented MaxProX100 TMS pulse
The spectra contain noise in the high frequency range above 100 kHz, which are significantly reduced by filtering. The transistors' switching noise with fundamental frequency of 300 kHz is visible in the spectra of the coil voltage and E-field.

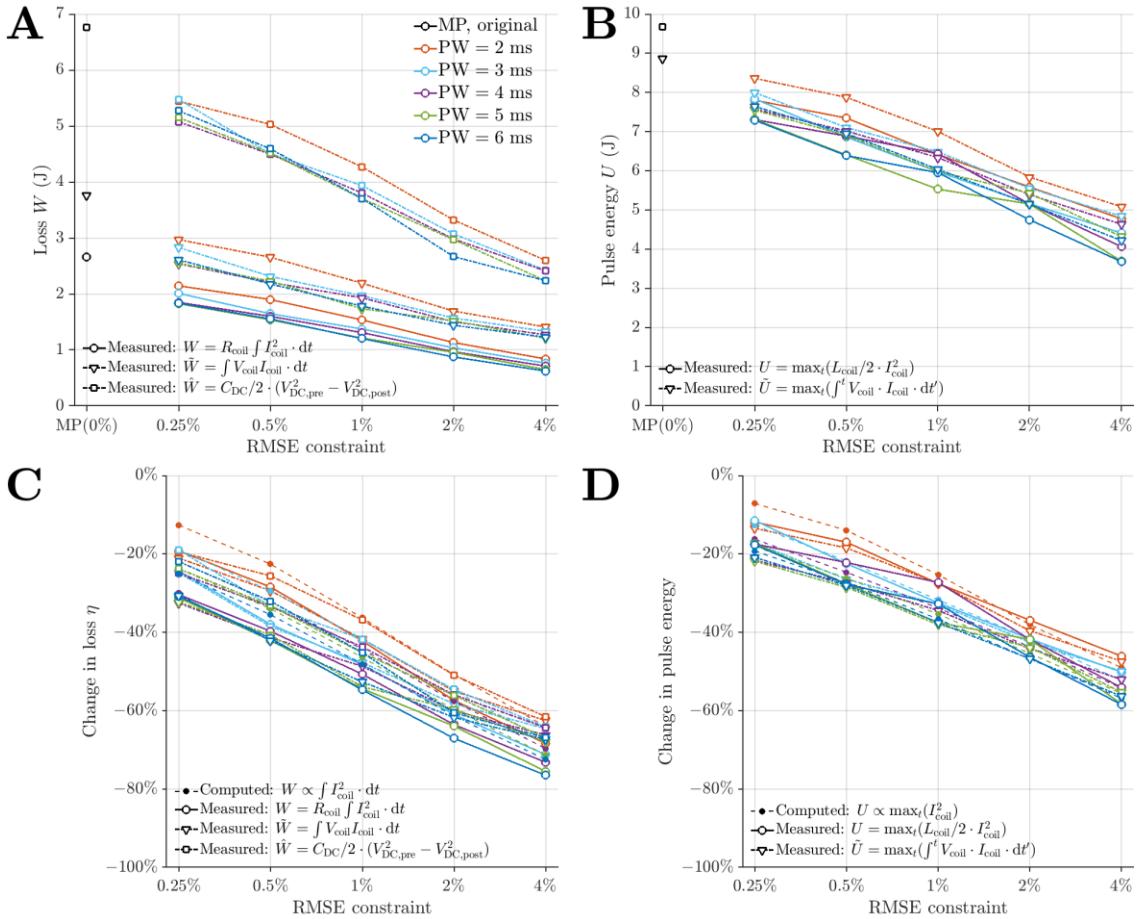

Figure S12: Losses and pulse energy of optimized pulses and original TMS pulse
Similar to Figure 6, with results for all pulse duration.

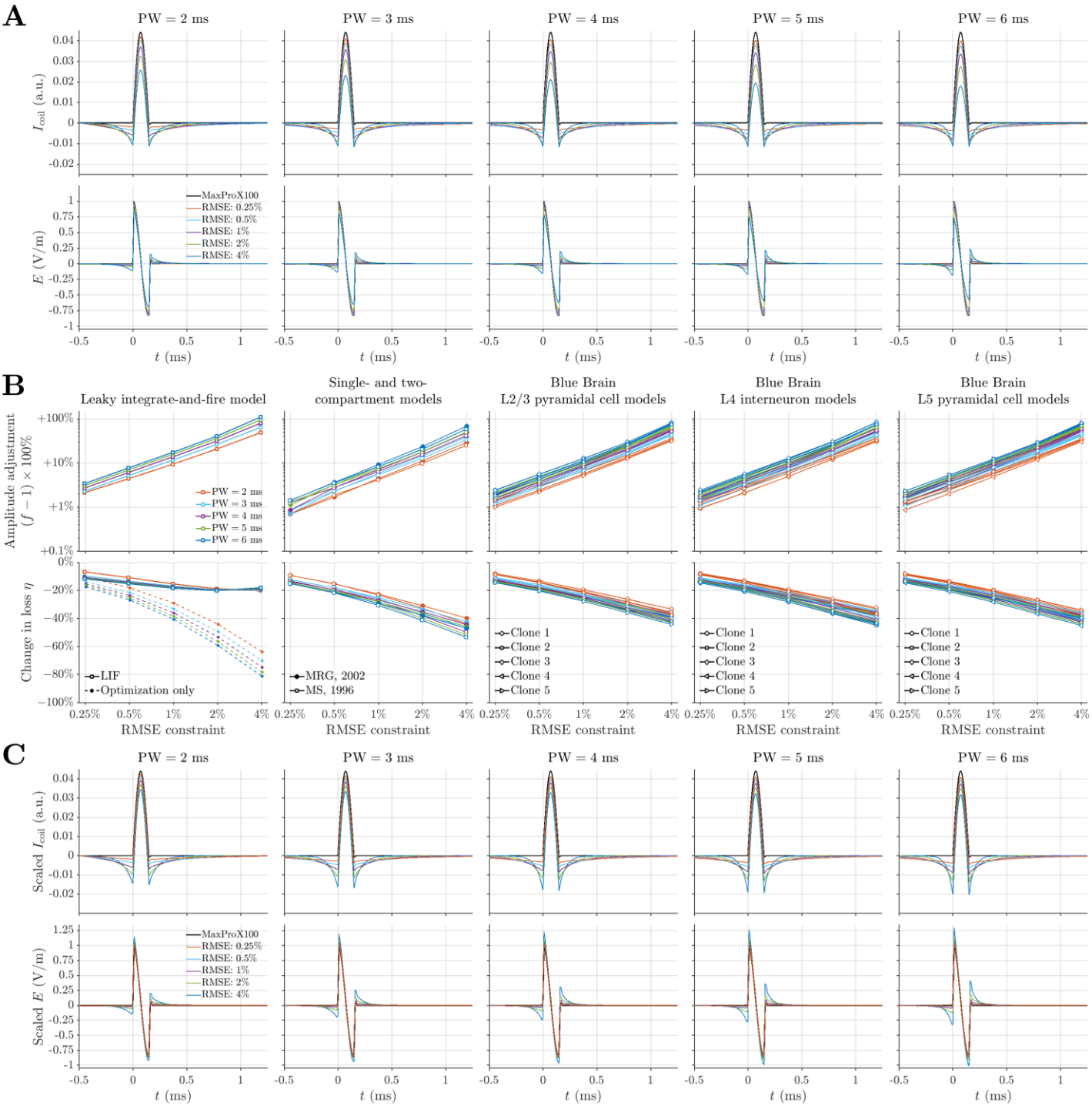

Figure S13: Waveform optimization, amplitude adjustments, and optimized waveforms for half-sine TMS pulses Similar format as Figure 2 for panel A and B and Figure 3 for Panel C, with only computed waveforms and without the coil voltage.

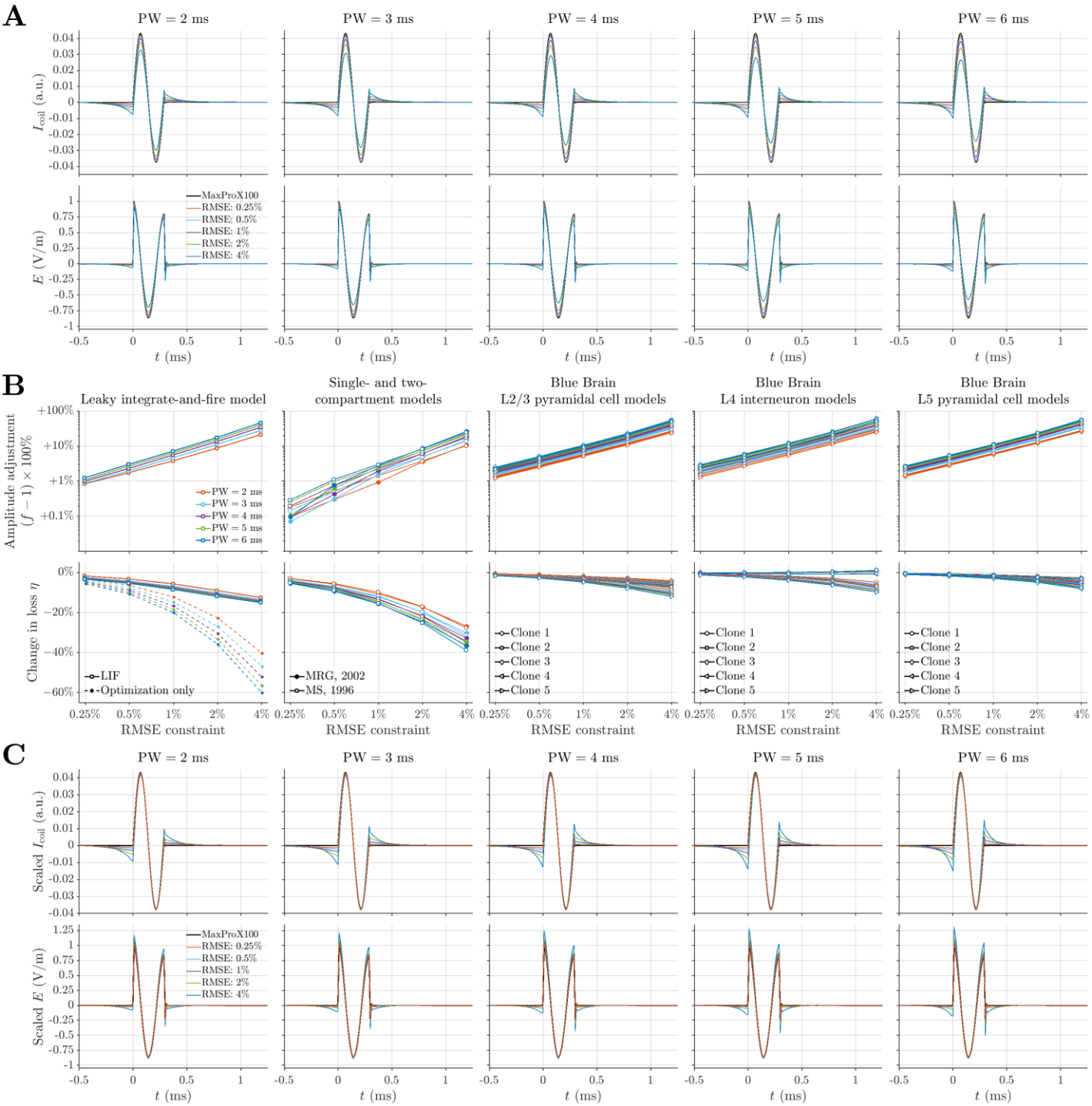

Figure S14: Waveform optimization, amplitude adjustments, and optimized waveforms for biphasic TMS pulses
Similar format as Figure S13, with different scale for the vertical axes in panel B for better visualization.